Master of Science Thesis
HT2020

Measuring T1 using MP2RAGE in Human Brain at 7T – Effect of B1+ and Inversion Pulse Efficiency

Mustafa Kadhim

Supervisors

Gunther Helms and Hampus Olsson

Medical Radiation Physics, Lund
Faculty of Science
Lund University
www.msf.lu.se

Abstract

Introduction: The MP2RAGE technique has become popular for structural MRI at ultra-high fields. The core idea behind MP2RAGE is to reduce the influence of flip angle inhomogeneity (B_1^+), proton density and T2* by calculating the regularized signed ratio of two complex MP-RAGE images acquired at different inversion times (TI) within the cycle. From this MP2RAGE signal, the underlying T1 relaxation time can be determined by means of a look-up table obtained by forward signal modelling. Nonetheless, persistent B_1^+ influence on MP2RAGE may be observed which can reduce the accuracy of the calculated T1 maps. An additional factor that might influence the estimated T1 is the efficiency of the adiabatic inversion pulse.

To study (and potentially mitigate) the influence of these variables, the dynamics of longitudinal magnetization during the cycle is simulated. The sensitivity of a given (and later modified) MP2RAGE protocol to B_1^+ is studied. The efficiency of the inversion pulse is estimated for different adiabatic pulses through both experiments and simulations.

Methods: Healthy adult subjects were examined on a 7T MR system using a dual-transmit head coil with a 32-channel receive array. The standard MP2RAGE protocol featured flip angles of $\alpha_1/\alpha_2 = 5^o/3^o$, TR= 6.8 ms, TI_1/TI_2 = 900/2750 ms, turbo factor TF=256, and a 5000 ms cycle duration. A DREAM sequence protocol with preparation flip angles of 25°,40°,60°,90° was used for B_1^+ mapping.

To study changes in inversion efficiency, f_{inv}, due to a spatially varying B_1^+ field, the maximum amplitude of the inversion pulse (B_1-max) was varied between 3 µT and 20 µT while keeping the pulse duration constant. To explore potential improvements in f_{inv} and residual B_1^+ bias respectively, the standard "Full adiabatic" inversion pulse was replaced by a FOCI pulse and the flip angles were changed to $\alpha_1/\alpha_2 = 4^o/5^o$. Simulations were performed in Python and T1-mapping in MATLAB using a script provided by the authors of MP2RAGE.

Results: Simulation of the standard protocol showed optimal T1 accuracy when utilizing a separate B_1^+ map and an inversion factor of 0.94 for the "adiabatic full" inversion pulse at B_1-max =18 µT. At B_1-max = 6 µT, f_{inv} was as low as 0.8. The inversion efficiency increased across the brain with increasing B_1^+. The inversion efficiency also seems to increase with B_1-max. An empirical dependence of f_{inv} on B_1^+ was derived, by which the accuracy of the T1-maps can be improved.

Additionally, the FOCI pulse yielded higher inversion efficiency at low B_1^+ regions in cerebellum and temporal lobes. Lastly, a higher second flip angle seems to result in T1-maps/MP2RAGE images that are less susceptible to B_1^+ inhomogeneity.

Discussion: The influence of B_1^+ inhomogeneity on a high-resolution MP2RAGE protocol at 7T was studied by simulation and experiment. Separately acquired B_1^+-maps improved the accuracy of T1. In particular, the efficiency of the standard "Full adiabatic" inversion pulse depended on B_1^+ and the chosen B_1-max. A similar investigation has been performed by Hagberg et al. at 9.4T. Notwithstanding better performance of the FOCI pulse in low- B_1^+ regions of the brain, B_1-max of the "Full adiabatic" pulse should be chosen as high as possible. The results prepare for further optimization of the MP2RAGE protocol and T1-mapping at UHF.

Popular scientific summary in Swedish

Den mänskliga hjärnan är ett anmärkningsvärt organ som formar våra mest komplexa tankar och medvetande. Ändå består den huvudsakligen av två typer av vävnader och en vätska, d.v.s. vit vävnad, (WM), grå vävnad (GM) och cerebrospinalvätska (CSF). Vit substans finns framför allt i de segment i centrala nervsystemet (CNS) som består av myeliniserade axoner och möjliggör långväga kommunikation mellan flera områden av grå vävnad samt överföring av nervimpulser mellan axoner i hjärnan. Grå vävnad å andra sidan kännetecknar de områden av hjärnan där neurala cellkroppar (soma) är belägna. När det gäller CSF sker dess produktion i kammarna där den absorberas av blodomloppet, vilket möjliggör transport av näring till olika delar av hjärnan och ryggmärgen.

Dessa olika vävnader har olika biofysiska egenskaper vilket inom MR-avbildning (MRI) kan utnyttjas för att skilja mellan dem. Sådana egenskaper är till exempel den longitudinella relaxationstiden (T1), den transversella relaxationstiden (T2), den effektiva transversella relaxationstiden (T2*) och protondensiteten (PD). T1 är relaterad till koncentrationen av myeliniserade axoner, järn och makromolekyler i hjärnan, vilket gör den värdefull för strukturell MRI. Speciellt för undersökningar av atrofi vid neurodegenerativa sjukdomar (Alzheimers, Parkinsons etc.) i hjärnan. I detta arbete fokuserar vi på att bestämma T1-relaxationstiden i WM, GM och CSF genom att utnyttja ett ultrahögt magnetiskt fält (UHF) på 7 T. Den höga magnetfältsstyrkan underlättar avbildning av anatomiska strukturer samt undersökning av patologiska förändringar i hjärnan. Dock så lider UHF av ökad inhomogenitet hos både de mottagande B_1^- och sändande B_1^+ -fälten vilket inducerar spatiala variationer i bildintensiteten.

För att mildra denna variation har en viss teknik fått uppmärksamhet inom strukturell MR på ultrahöga fält ($\geq$ 7T). Denna teknik är Magnetization Prepared 2 Rapid Acquisition Gradient Echoes (MP2RAGE), vilket är en mer sofistikerad utveckling av MPRAGE-sekvensen. Tanken bakom MP2RAGE är att minska påverkan av flippvinkelinhomogeniteter på grund av den ökade inhomogeniteten hos B_1^+ samt signalvariationer p.ga. B_1^-. Dessutom kan signalvariationer p.g.a. skillnader i protondensitet och T2* elimineras. Detta görs genom att beräkna det regelbundna signalförhållandet mellan två komplexa MPRAGE-bilder som erhållits vid olika inversionstider (TI) inom en cykel. Av denna anledning är MP2RAGE sekvensen av intresse i detta arbete. Dock, trots användning av MP2RAGE-sekvensen, så kan kvarvarande effekter av variationer i B_1^+ fortfarande observeras. Detta kan resultera i minskad noggrannhet i de beräknade T1-värdena. En annan faktor som kan påverka noggrannheten i uppskattad T1 är inversionspulsens effektivitet.

Således, vårt mål med detta arbete var att bestämma inversionseffektivitetsfaktorn på en 7T Philips MR-kamera samt undersöka möjligheten att förbättra noggrannheten i de uppskattade T1-värdena genom att använda en lokal flippvinkelkarta. Dessutom har vi skapat ett simuleringsverktyg för att underlätta utvärderingen och förståelsen av utvecklingen av den longitudinella magnetiseringen under en MPRAGE eller MP2RAGE sekvens. Verktyget kan även användas till att simulera fler än två utläsningståg med arbiträra flippvinklar. Även hur signalen och den longitudinella magnetiseringen påverkas på grund av ovan nämnda faktorer undersöktes. Slutligen genomfördes en jämförelse mellan två inversionspulser för att studera deras inverkan på MP2RAGE-bilderna och T1-uppskattningen.

Acknowledgement

Foremost, I would like to start by expressing my gratitude to my supervisors, **Gunther Helms** (*Ph.D. Swedish National 7T Facility, Senior Lecturer, Medical Radiation Physics, Lund*) and **Hampus Olsson** (*Doctoral student, Medical Radiation Physics, Lund*), for their contribution, encouragement, guidance, allowing me to have fun, and giving me the opportunity to work on such an interesting project. Thank you for sharing your expertise and knowledge with me.

My sincere thanks also goes to the **Michael Ljungberg** (*PhD, professor, head of office at Medical Radiation Physics, Lund*), **Sofie Ceberg** (*PhD, Assoc. Senior Univ. Lecturer Department of Medical Radiation Physics, Lund*), and **Linda Knutsson** (*Ph.D., Professor, Medical Radiation Physics, Lund*) for their support, guidance, and making sure that I'm feeling well during the stressful period of writing a thesis work.

I would like to thank my classmates for making the journey of becoming a medical physicist full of fun memories and unreasonable amount of coffee and fika.

Lastly but definitely not the least, big thanks to my family and friends for being there for me during the strange times of living through a pandemic while trying to finish this thesis work.

Once again, THANK YOU ALL!

List of contents

Abbreviations

MRI	Magnetic resonance imaging.
WM	White matter.
GM	Grey matter.
CSF	Cerebrospinal fluid.
CNS	Central nervous system.
RF	Radiofrequency.
TI	Time of inversion.
T1	Longitudinal relaxation time.
$\mathbf{M_z}$	Net longitudinal magnetization vector.
$\mathbf{B_1^+}$	Transmit RF magnetic field component.
B_1-max	The maximum amplitude of the inversion RF pulse.
$\mathbf{B_1^{+*}}$	Relative B_1^+ of selected ROIs.
$\mathbf{B_{1}}_{ref}$	Reference B_1-max: 18µT.
FA	Flip angle.
$\boldsymbol{f}_{\mathbf{inv}}$	Inversion efficiency.
UHF	Ultra-high field.
SNR	Signal-to-noise ratio.
SAR	Specific absorption rate.
MPRAGE	Magnetization Prepared RApid Acquisition of Gradient Echoes.
MP2RAGE	Magnetization Prepared 2 RApid Acquisitions of Gradient Echoes.

1 Introduction

The human brain is a remarkable organ, responsible for our most complex thoughts and our greatest achievements. Yet, it consists mainly of two kinds of tissues and a surrounding fluid: white matter (**WM**), grey matter (**GM**), and the cerebrospinal fluid (**CSF**). White matter is found in the segments of the central nervous system (CNS) that consists primarily of myelinated axons, which enable the long-range communication between several grey matter areas, along with transmitting nerve impulses among axons in the brain. Grey matter on the other hand makes up the area of the brain where neuronal cell bodies (soma) are located. As for the cerebrospinal fluid, its production takes place in the ventricles and is later absorbed by the bloodstream, allowing for the transportation of nutrition to different sections of the brain and the spinal cord.

These different components have different biophysical properties that in the field of MR imaging can be exploited to distinguish them. Examples of such properties are the longitudinal magnetization relaxation time (**T1**), the transverse magnetization relaxation time (**T2**), the effective transverse magnetization relaxation time (T2*) and the proton-spin-density (**PD**). T1 is related to the concentration of myelinated axons, nonheme iron and the quantity of macromolecules, making it of value for structural MRI [1]. It is especially useful for examinations of atrophy in neurodegenerative diseases (Alzheimer's, Parkinson's, etc.) in the brain (ref). The focus of this thesis is determining the T1 relaxation time in WM, GM, and CSF.

T1 represents how fast the net longitudinal magnetization ($\mathbf{M_z}$) pointing along the same direction as the static magnetic field in the MRI scanner ($\mathbf{B_0}$), relaxes back to its initial state ($\mathbf{M_0}$) post excitation by a radiofrequency (**RF**) pulse. Tissues acquiring short T1-values appear brighter (high signal) in T1-weighted MR images than tissues with long T1. However, the T1-values are not universal for the tissues but also dependent on the strength of the magnetic field in the MRI scanner [2]. In this thesis, a 7T Philips MRI scanner is used to obtain all image data.

In the field of MR imaging, there are many different pulse sequences that enable achieving multiple types of diagnostic images dependent on the purpose of examination. One of these sequences that have recently gained popularity is the Magnetization Prepared 2 Rapid Acquisition Gradient Echoes (**MP2RAGE**), which is a more sophisticated extension of the MPRAGE sequence [3]. The reason behind the admiration of MP2RAGE is its ability to produce diagnostic images with decreased dependency on the receive/transmit $\mathbf{B_1^-/B_1^+}$ fields, PD, and $\mathbf{T_2^*}$ [4]. This is of importance when dealing with ultra-high magnetic fields ($\geq$ 7T), as the increased inhomogeneity of both the receive B_1^- and transmit $\mathbf{B_1^+}$ fields induce variations in the diagnostic image intensities while T_2^* induces a spatial blurring effect [3]. Therefore, MP2RAGE is the sequence of interest in this thesis.

The inhomogeneity of the local flip angles across the brain range from 40% to 140% of the nominal flip angle [5]. In which may lead to undesired image intensity variations and inaccurate

T1-determination (for certain T1-mapping techniques). Nonetheless, the T1-values can be derived by a lookup table from the purely T1-weighted image of a self-referenced inversion recovery experiment (MP2RAGE). The look-up Table enables conducting T1-mapping where the MP2RAGE intensity values are translated to corresponding T1-values.

Moreover, the MP2RAGE image intensity depends on certain factors; the inversion time (**TI)**, the inverted fraction of M_0 (which in return depends on the inversion efficiency). Along with the length and flip angles of the two readout trains (**RAGE**).

Thus, our objective was to determine the inversion efficiency factor ($\boldsymbol{f_{inv}}$) on the 7T Philips scanner and investigate the possibility of improving the accuracy of the T1-values by utilizing a local flip angle map. Moreover, we created a simulation tool to facilitate the evaluation and understanding of the evolution of M_z during an MP-RAGE or MP2RAGE sequence. The tool can also be used to model a sequence with an arbitrary number of RAGE trains (“ MPXRAGE”) and how the signal, along with M_z, is influenced due to the above-mentioned factors. Lastly, a comparison between two adiabatic inversion pulses, namely the “Full Adiabatic” pulse and the frequency offset corrected inversion (FOCI) pulse, was conducted to study their impact on the MP2RAGE image and T1 estimation.

2 Theory

2.1 T1 Relaxation

The T1-relaxation of the net longitudinal magnetization (**M_z**) is described by the Bloch equations as a first order exponential given in Eq. (1). The special case in Eq. (1) indicates that at time zero, Mz = 0 ("saturation") and around the time T1, the longitudinal magnetization has restored around 63% of its equilibrium value (**M_0**).

$$M_z(t) = M_0 \left(1 - e^{-\frac{t}{T1}}\right). \quad (1)$$

Where *t* stands for the time after a 90° excitation.

As the nuclear dipoles excited by the radiofrequency pulse (**RF**) seek alignment with the parallel static magnetic field in the MRI scanner (**B_0**). To project down the net magnetization vector M on the *xy*-plane, an RF-pulse (**B_1**) is required to be transmitted with the Larmor frequency and perpendicular to the B_0 vector.

The T1-relaxation can also be seen as a restoration of thermal equilibrium. Since molecules and atoms transfer the obtained spin excitation energy from the RF pulse to their environment to return to their equilibrium state M_0. For the energy transfer to take place, a stimulation near the Larmor frequency is required. This normally occurs in a liquid material by the rotation of molecules where the dipole moment of the other protons induces oscillating fields near the Larmor frequency [6]. Different magnetic field strengths give rise to different T1 values. This is a consequence of the influence of B_0 on the spin and interaction with macromolecules.

A simple technique to determine the T1-value of a certain biological material/tissue is the Inversion Recovery (**IR**) pulse sequence. The IR sequence starts by sending a 180°-RF pulse to flip the M_z vector from + M_z to - M_z. Immediately after, the T1-relaxation starts taking place in the material to align the M_z vector parallel to the B_0 field. As the tissue is undergoing T1-relaxation, a spin echo readout pulse (90°-RF pulse) is applied at an inversion time (**TI**) to detect the signal as the M_z vector approaches its equilibrium value. The T1-value is later estimated by taking advantage of the selected TI-value suppressing the signal from the tissue. From the Bloch equations, the behavior of M_z during an IR sequence can be expressed by Eq. (2).

$$M_z(TI) = M_0 \left(1 - 2e^{-\frac{TI}{T1}}\right). \quad (2)$$

Where *TI* is the inversion time. It can be modified to suppress the signal of a selected tissue with a specific T1-value.

The equation is a simplified description based on the assumptions; full inversion of M_z, the time of repetition (**TR)** is long enough for the M_z vector of a tissue to fully recover to M_0, the time of echo (**TE**) is always the same for the selected TI, and a 90°-RF pulse is applied. In Fig.1 an illustration of the behavior of M_z immediately after a spin echo readout (90°-RF pulse) is given in A) and during an IR pulse sequence (180°-RF inversion pulse) is given in B).

The parameter T1 can be derived by utilizing two images acquired at different TI. By acquiring two images, the M_z vector with respect to different TI can be plotted and T1 can be found by an exponential fit (more than two images) or solved directly. The obtained T1-value can in turn be substituted back into Eq. (2) to acquire M_0. Thus, T1 and M_0 can technically be achieved from only two images at different TI. Another approach to obtain T1 is based on the division of the two images at different TI to attain the following expression.

$$\left(\frac{M_z(TI_2)}{M_z(TI_1)}\right) = \left(\frac{1-2e^{-\frac{TI_2}{T_1}}}{1-2e^{-\frac{TI_1}{T_1}}}\right). \tag{3}$$

Since the left-hand side of the expression corresponds to a given value and the only unknown variable on the right-hand side is T1, its value can then be varied until a suitable T1 value is found to satisfy the left-hand side of the expression given above. Additionally, the M_0 term cancels out.

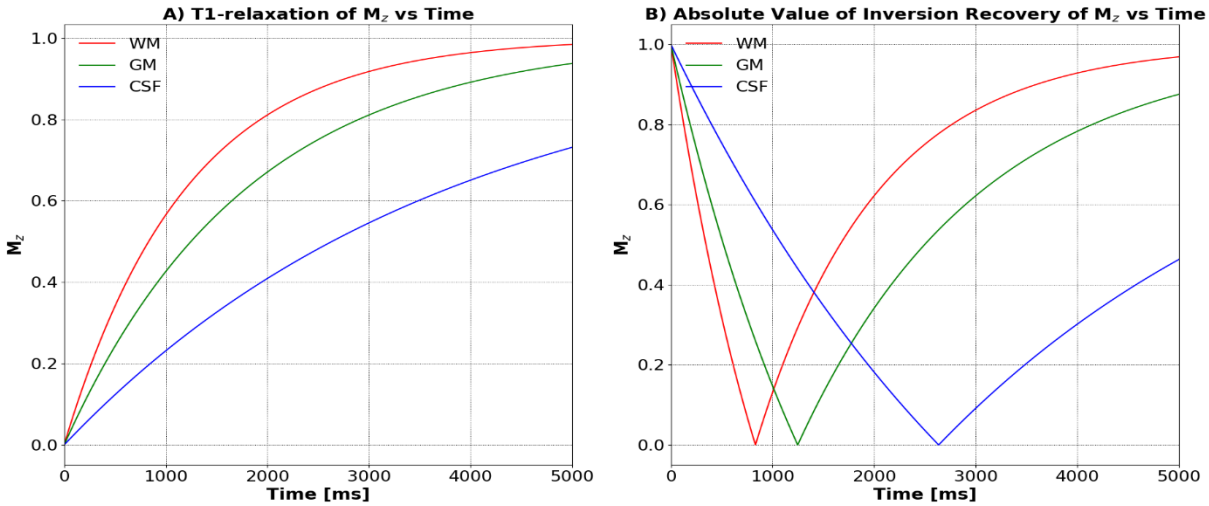

Fig. 1. A) Illustration of the T1-relaxation of M_z in white matter (WM), grey matter (GM), and Cerebrospinal fluid (CSF) post excitation by a spin echo readout pulse (90° -RF pulse). As observed, a proper selected TI leads to enhanced contrast between the tissues. B) T1-relaxation of the absolute value of M_z (magnitude) in an inversion recovery (IR) pulse sequence post inversion by a 180°-RF pulse in the same tissues. The M_0 values for the different tissues are set to be equal 1.0 in both figures for simplicity. The selected T1 for WM, GM, and CSF are 1200, 1800 and 3800 respectively valid for 7 Tesla [2].

Moreover, Fig.1.B) illustrates the challenge of knowing the T1-value of the tissues as the sign of the magnitude of the signal is always positive. As observed, CSF will appear brighter than WM if TI is short, while it appears darker for a longer selected TI. Consequently, misjudgment of a tissue's T1-property might occur if improper TI is chosen. Thus, there is a need for an approach offering signed inversion recovery imaging.

2.2 Working with 7T MRI Scanners

The recent developments in the engineering of MRI scanners opened the door for utilizing UHF strengths ($\geq$ 7T) in clinical/research applications, to further investigate the anatomical structures and pathological processes in the brain with greater detail. In comparison to using lower magnetic field strengths (3T, 1.5T), the increase in the magnetic field strength results in a change of the biophysical parameter (T1 and T2) values in the test subject. As the parameters are correlated to the strength of the magnetic field over the rather small range of B_0 of human MR scanners. For instance, the T1-parameter becomes longer with higher field strengths while the T2 and $T2^*$ become shorter. This behavior can be either beneficial or hampering depending on the aim and methodology of the study.

Some of the immediate improvements that are associated with 7T (UHF) scanners are the following:

1. Increased signal-to-noise ratio (SNR) and spatial resolution: The SNR increases linearly with the field strength (higher spin polarization of tissues) and leads to higher detection rate of fine anatomical structures by reducing the noise level in images. Additionally, SNR can be utilized to reduce the scanning time to evade motion artefacts and improve tissue segmentation [7]. Increased spatial resolution facilitates observation of pathological processes and anatomical structures that are hardly observed in lower field scanners and could have a huge impact in the fields of MRI angiography and neuroscientific imaging for detecting diseases in early stages [8].

Some of the disadvantages in our case (beside increased B_1^+ inhomogeneity) that are associated with 7T (UHF) scanners are the following:

1. Increased susceptibility sensitivity: the following results in undesired increase in susceptibility artefacts (geometric distortion) originated from local magnetic field inhomogeneity [9]. Leading to decreased image quality. Nonetheless, it can be exploited in susceptibility weighted imaging.

2. Increased specific absorption rate (SAR): more tissue heating by induced electrical currents in the body originating from the interaction of high energy RF pulses. Based on physics, the SAR value shall be increasing quadratically for field strengths higher than 3T, but it has been shown that it increase linearly above 3T [10]. However, for a linear increase of SAR, an increased sequence timing is required (due to longer T1).

3. Acute physiological side-effects depending on B_0 strengths: Associated temporary side-effects such as nausea, dizziness, peripheral nerve stimulation (PNS), headache, inconsistent movement, metallic taste and light flashes are more common to be experienced by subjects in a 7T scanner than lower field scanners [11][12].

4. Increased Chemical shift artefact: The following might be considered to be beneficial for examining fat saturation of tissues or in the field of MR spectroscopy. However, the increased chemical shift results in a water/fat misregistration, reducing the clinical value of the image [13]. An additional consequence of the above, is the decrease of the T1-value in fat rich regions of the tissue [12].

5. Specifically designed protocols and modification of components: more efficient RF coils design are required for UHF scanners to avoid B_1^+ spatial inhomogeneities [14]. Still, due to the many challenges mentioned above, optimized protocols are required for UHF MR scanners to facilitate image interpretation by the clinical staff (radiologists).

2.3 MPRAGE

The Magnetization Prepared RApid Gradient Echo (MPRAGE) is an MRI sequence, used to obtain high-resolution, high-contrast T1-weighted 3D images within a clinically suitable time [15][16]. The sequence consists of three different intervals: The magnetization preparation interval, the acquisition interval, and the magnetization recovery interval. The following is illustrated below in Fig.2.
The magnetization preparation interval initiates by the inversion of the M_z vector from $+M_z$ to $-M_z$ through the employment of a non-selective 180°-RF pulse. Next, the M_z vector relaxes via T1-relaxation back towards M_0 during an inversion time, TI. At the time TI, the signal acquisition initiates by a rapid acquisition gradient echo (RAGE) train with constant low flip angles, α_1^o and short TR. The signal acquisition takes place throughout the k-space. However, as a simplification, the signal acquisition can be assumed to occur at the center of k-space. Following the RAGE-block, the M_z vector recovers via T1-relaxation over the time TD. The cycle duration is given by $MPRAGE_{TR}$.

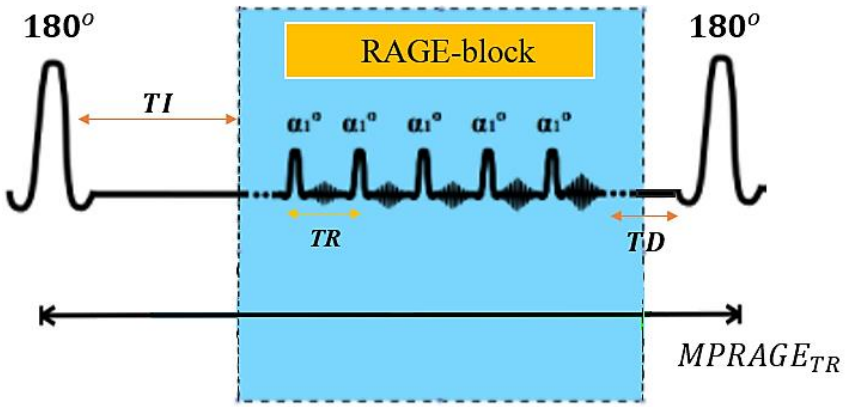

Fig. 2. Schematic MPRAGE sequence illustration where TI represents the time of relaxation between the center of the non-selective inversion pulse (180°-RF pulse) and the read-out of the central k-space line in the RAGE train, TR is the time between consecutive excitations, α_1^o is the readout flip angle, and TD is the relaxation time between the RAGE train and the beginning of a new inversion at time $MPRAGE_{TR}$.

In addition to the above, the sequence needs to achieve a **steady-state** through periodic repetition of the sequence cycle multiple times, since M_z will be less than M_0 at the end of the cycle as a consequence of the RAGE-block and the inversion pulse. In which may lead to inaccurate signal readouts based on the effect of having a different start point for M_z as the next cycle initiates (defined as M_z (start of cycle)). A steady-state imply a constant magnetization/signal state at some point in the sequence that can be utilized to acquire the MPRAGE images at an M_z level distinct from M_0 [16]. The mechanism behind the steady-state phenomena is the rapid employment of readout RF-pulses with angle α_1^o, that lead to a balance between the magnitude of M_z (restored by T1-relaxation) and M_{xy} (restored by α_1^o) allowing a balance of the net magnetization vector, hence, a steady-state M_{ss}. Arising from not allowing a full recovery of M_z between the short TR.

One can think of M_z as a reservoir to the signal that is wisely being exploited during each TR for small α^o, instead of fully emptying the reservoir by a 90°-RF pulse. Where the next time an RF pulse is employed, M_z will be much shorter than before, contributing to a reduced signal (shorter M_{xy} vector) [17]. Thus, low flip angle sequences combined with fast GE techniques offer higher signal at shorter TR than sequences with 90° pulses [18].

The TI and TD parameters are of importance for the MPRAGE sequence as they may be used for contrast control between different tissues [16]. The MPRAGE image contrast is highly dependent on the difference in the T1-value of the tissues. Nonetheless, proton-spin density (M_0) variations, $T2^*$ effects, and an amplified inhomogeneity of the B_1^- and B_1^+ fields may reduce the image quality when MPRAGE is operated on UHF scanners [3].

2.4 MP2RAGE

Magnetization Prepared 2 Rapid Acquisition Gradient Echoes (MP2RAGE) is a further development of the MPRAGE sequence, introduced to overcome the increased B_1^+ and B_1^- field inhomogeneities at UHF that are too large for post processing intensity algorithms to adjust for [19]. The core idea behind MP2RAGE is to take advantage of the ratio of two sorts of image volumes (3D image) taken at different inversion times (TI), a 3D T1-weighted (T1w) volume and a 3D proton density weighted (PDw) volume, to obtain more uniform T1w images that are independent of B_1^-, B_1^+, $T2^*$, and proton density ρ, as given in the expression below [4].

$$S_p = \frac{S_{MP}}{S_{GE}} = \frac{\rho}{\rho} \cdot \frac{M_{MP}}{M_{GE}} \cdot \frac{|\boldsymbol{B_1^-}| \sin(V|\boldsymbol{B_1^+}|\gamma\tau) e^{-\left(\frac{TE}{T2^*}\right)}}{|\boldsymbol{B_1^-}| \sin(V|\boldsymbol{B_1^+}|\gamma\tau) e^{-\left(\frac{TE}{T2^*}\right)}} = \frac{M_{MP}}{M_{GE}} \quad (4)$$

Here S_P is the pixel intensity, ρ is the proton density, $\boldsymbol{B_1^-}$ is the receiver RF coil sensitivity, γ is the gyromagnetic ratio, τ is the equivalent duration of a square pulse, V is a scaling factor, and M_{MP}/M_{GE} are the longitudinal magnetization in MPRAGE and the added GE-block respectively. As observed, the flip angle of a square pulse $\alpha^o = V|\boldsymbol{B_1^+}|\gamma\tau$, is proportional to the magnitude of the transmit field, B_1^+ [4]. The above holds for a constant spatial resolution (bandwidth) for the acquisition of MPRAGE and GR.

A simplified illustration of the MP2RAGE sequence is presented in Fig.3. The image volumes are obtained by RAGE readouts following an inversion pulse (180°-RF pulse) inverting M_z to $-M_z$. Each GE train is acquired at a specific low flip angle, α_1^o or α_2^o, short repetition time, TR (between two excitations within the same block), and an assigned TI-value outlining the time from the middle of the inversion pulse peak to the readout of the line through the center of the k-space in the first/second-phase encoding direction. TR is often identical in both GE blocks together with the number of excitations, *n*, to achieve similar RAGE train lengths.

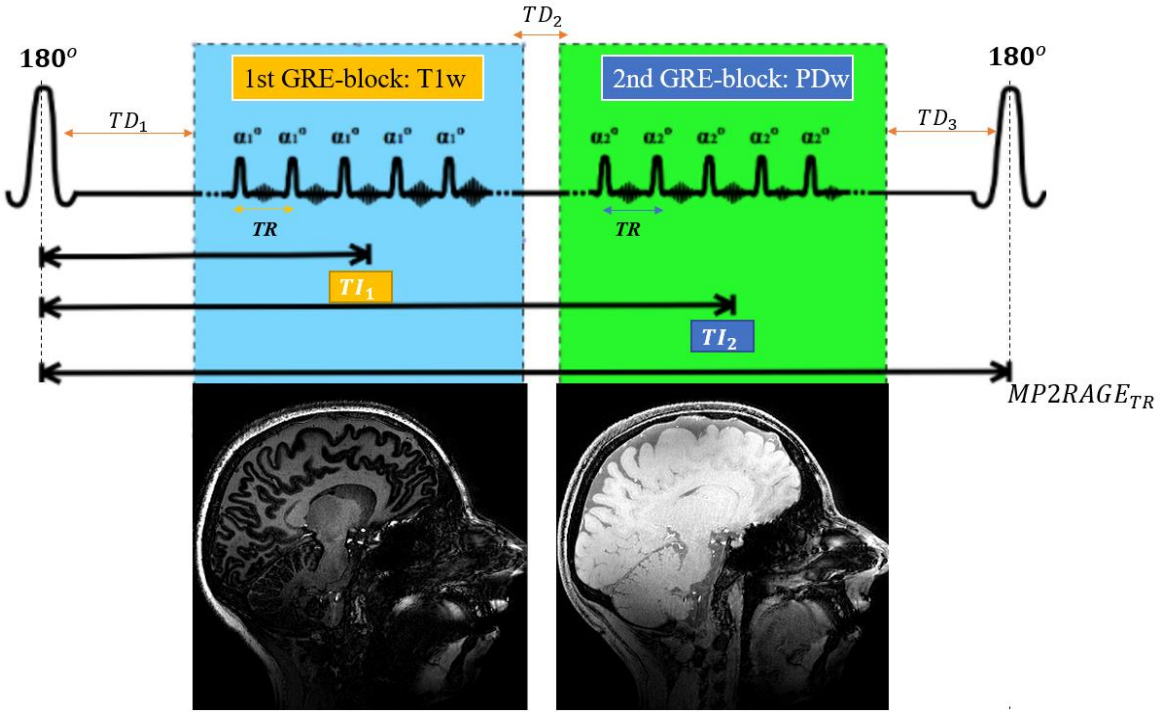

Fig. 3. Schematic MP2RAGE sequence illustration where TD represents the time of T1-relaxation between the different phases of the MP2RAGE cycle ($MP2RAGE_{TR}$), TI1 and TI2 are the inversion times estimated from the middle of the inversion pulse peak to the center of the k-space line in the second-phase encoding direction and α_1^o / α_2^o are the flip angles for respective block.

Specifically for MP2RAGE, the intensity is calculated from the complex signals S_{TI_1} and S_{TI_2} by the mathematical formula in Eq. (5) [3]. On the Philips scanner, two images with real and imaginary signal components are stored, from which $\boldsymbol{S}_{MP2RAGE}$ is calculated.

$$\boldsymbol{S}_{MP2RAGE} = \frac{real\left(S_{TI_1} \cdot S_{TI_2}^*\right)}{\left|S_{TI_1}\right|^2 + \left|S_{TI_2}\right|^2} = \frac{real\left(S_{TI_1}\right)real\left(S_{TI_2}\right) + imag\left(S_{TI_1}\right)imag\left(S_{TI_2}\right)}{real\left(S_{TI_1}\right)^2 + imag\left(S_{TI_1}\right)^2 + real\left(S_{TI_2}\right)^2 + imag\left(S_{TI_2}\right)^2}, \quad (5)$$

where $S_{TI_2}^*$ represents the complex conjugate of the images.

To further understand MP2RAGE, Eq. (5) can be rewritten in terms of the image magnitude and phase

$$\boldsymbol{S}_{MP2RAGE} = \frac{\frac{\left|S_{TI_1}\right|}{\left|S_{TI_2}\right|}\cos(\phi_1 - \phi_2)}{\frac{\left|S_{TI_1}\right|^2}{\left|S_{TI_2}\right|^2} + 1}. \quad (6)$$

where the $\cos(\phi_1 - \phi_2)$ term represents the phase difference between S_{TI_1} and S_{TI_2}.

The fraction S_{TI_1}/S_{TI_2} in Eq. (6) signifies the semi-quantitative properties of the MP2RAGE sequence, as local B_1^- and B_1^+ are cancelled out. Moreover, an improvement of the T1-weighting is observed due to mitigated inverse proton density weighting and $T2^*$ decay effect [3][16]. Additionally, the S_{TI_2} read out from positive M_z aids as a reference for the local signal phase in MP2RAGE.

In case the S_{TI_1} term is mainly obtained from the positive M_z, the phase difference $\phi_1 - \phi_2$ is close to 0 and the MP2RAGE signal is positive. And negative if read out from negative M_z due to a phase difference of π. This is advantageous as it offers an approach for signed inversion recovery imaging with gradient echo acquisition. Finally, a reduced phase noise level (more importantly for $S_{TI_2} \approx 0$) is achieved due to the $\cos(\phi_1 - \phi_2)$ term. Finally, the "+1" term in the denominator prevents the division by zero.

The obtained MP2RAGE images using Eq. (5) are presented in Fig.4. The values of $\boldsymbol{S}_{MP2RAGE}$ are bounded to [-0.5,0.5].

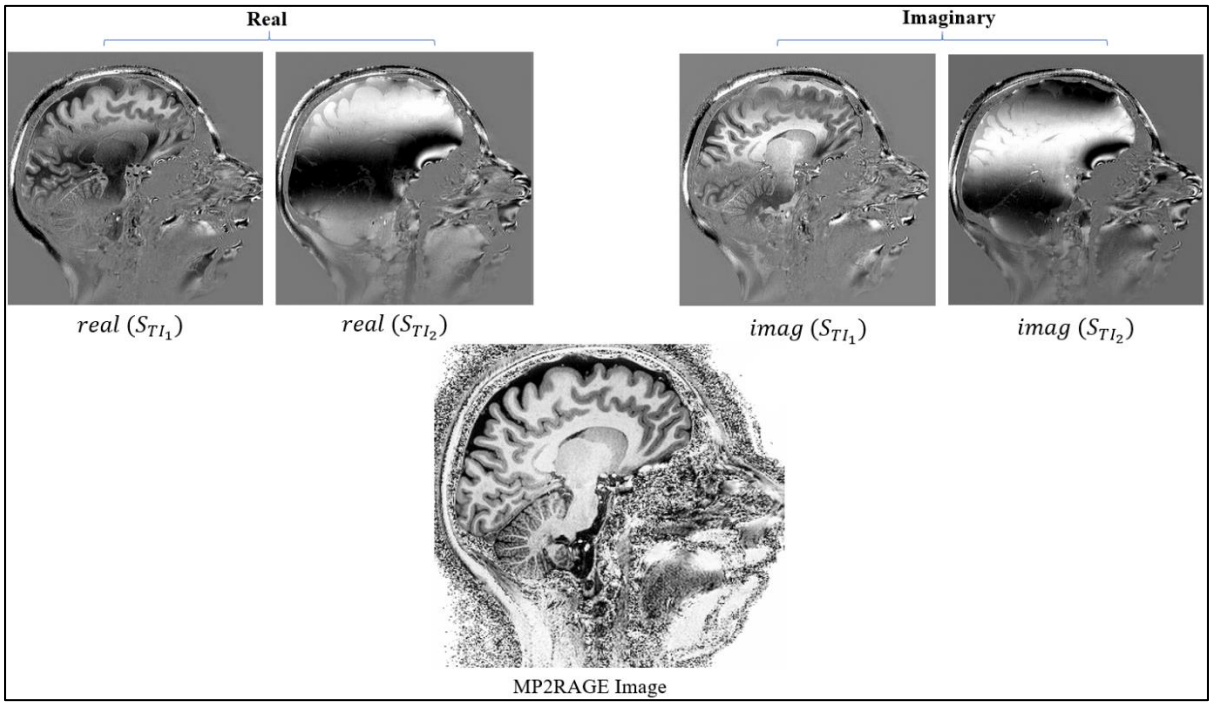

Fig. 4. The MP2RAGE image is determined by using both the imaginary and real image data along with Eq.(5). The $real(S_{TI_1})$ and $real(S_{TI_2})$ stand for the real volume 1 and 2. The same applies for the imaginary part.

As observed in Fig.4, the images are purely T1-weighted. In the calculated MP2RAGE from complex Philips images, the noise in air surrounding the brain in the resultant MP2RAGE image is high. This is a consequence of low signal in the dividing images which tends to amplify noise. On the other hand, the brain tissues are showcased with rich details and a desired contrast enabling thorough examination of the tissues. Later, these high quality MP2RAGE images can be exploited to create T1-maps or in segmentation of specific regions or tissues of the brain.

2.5 T1-Mapping

The idea behind T1-mapping is to be able to offer T1 quantification down to the pixel level of an MR image, where each pixel intensity represents the T1-value of the underlying voxel. One usually talks of T1 maps. As this will enable more in-depth studies of the tissue pathology and assessment of diseases. This technique can be employed within many branches of MR imaging. To illustrate how a T1-map looks, an example is presented in Fig.5.

There are several different methods to construct T1-maps. For our purpose, the construction of T1-maps builds upon forward modelling, combining knowledge of the image pixel value (calculated by a simulation), the assigned inversion efficiency (the inverted fraction of net M_z) and a local flip angle value to create a look-up table [3].

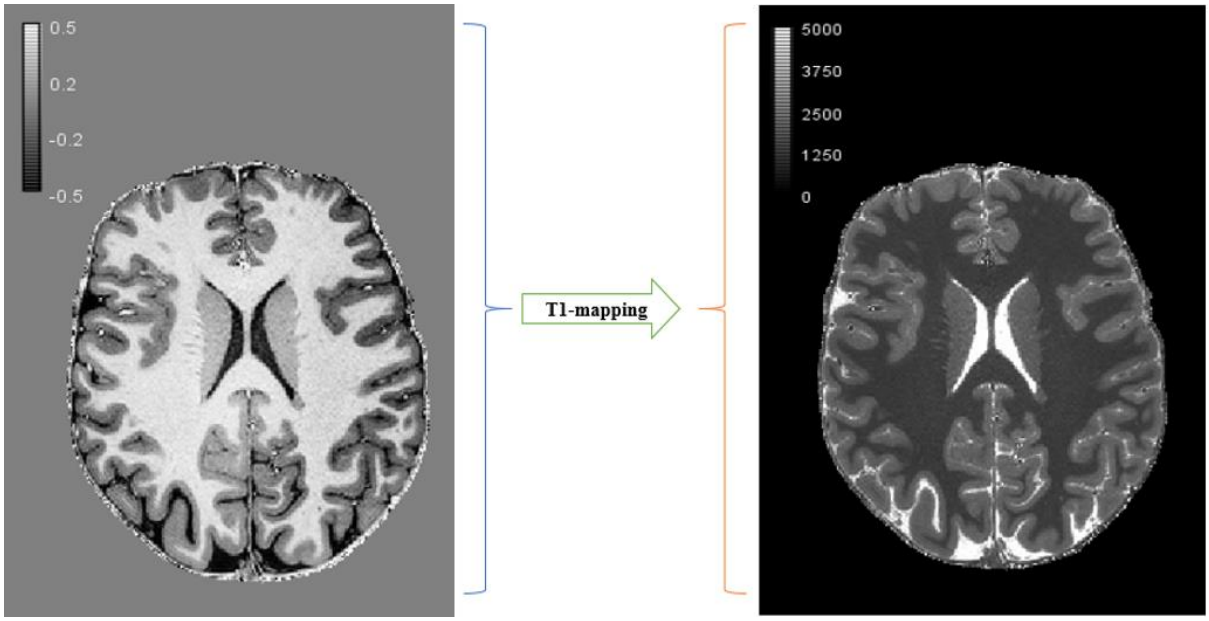

Fig. 5. T1-mapping applied to an MP2RAGE brain image with intensities between -0.5 and 0.5 where each pixel value in the output image reflects a T1-value in ms.

2.6 Simulation of MP2RAGE

2.6.1 Simulation of the M_z cycle

To gain further understanding regarding the MP2RAGE intensity dependence on the sequence parameters, a tool to simulate the dynamic of M_z during the cycle(s) of the sequence is needed. To do so, the cycle of the MP2RAGE sequence is first divided into few intervals where different processes take place, as shown in Fig.3.

1. **Interval 1**: the employment of the inversion pulse inverting the longitudinal magnetization from $+M_z$ to $-M_z$. The imperfect inversion is simply accounted for by replacing the $\cos(\pi)$term by the inversion efficiency factor, f_{inv} to obtain Eq. (7).

$$M_z^- = -M_z^+ \cdot f_{inv}\,, \tag{7}$$

where M_z^- is the start magnetization immediately after the adiabatic inversion.

Since the parameter f_{inv} is an empirical parameter, it can be modified to describe $M_z(0)$.

2. **Interval 2**: a waiting time TD_1 before the RAGE train is applied. During this time a T1-relaxation takes place enabling $-M_z$ to approach M_0, as given in Eq. (8).

$$M_z(t) = M_0 - (f_{inv}\, M_z(end\ of\ cycle) + M_0)\, e^{-\frac{t}{T_1}}, \tag{8}$$

where t is the time passed from the center of the inversion pulse, T_1 is the T1-value for selected tissue and $M_z(end\ of\ cycle)$ is the M_z value at the end of the cycle.

The $M_z(end\ of\ cycle)$ term is important to determine the steady-state. Additionally, if the waiting time ($t = TD_1$) is too long the value of M_z approaches M_0.

3. **Interval 3**: After TD_1, the first RAGE train is applied to obtain the first block representing the T1w images. During this process, equidistant spacing of excitations by the first flip angle, α_1^o at a certain TR for adjacent encoding steps are implemented. The excitation can be expressed according to Eq.(9). Moreover, a T1-relaxation take place in between the excitations which can be accounted for in the simulation according to Eq.(10). Hence, Interval 3 can be expressed as follows:

$$M_z^-(t) = M_z^+(t) \cdot \cos(\alpha_1^0)\,, \tag{9}$$

$$M_z^+(t + TR) = M_0 + (M_z^-(t) - M_0)\, e^{-\frac{TR}{T_1}}\,, \tag{10}$$

where M_z^+ is the M_z value during T1 relaxation and M_z^- is the M_z value immediately after excitation by α_1^0. In practice TR is much shorter than T1.

Based on the above equations, simulation of an MP2RAGE sequence becomes feasible. Since the same principle applies for the simulation of the remaining processes, the T1 relaxation during TD_2, the excitation process during the 2nd GE-block (α_2^o) and the T1 relaxation prior to the excitation (TD_3).

With linear phase encoding, the signals (S_{TI_1} and S_{TI_2}) used to calculate the MP2RAGE images are acquired in the middle of the RAGE train (TI_1 and TI_2) as it represents the center of the k-space [21][15].

The application of the RAGE trains leads M_z to converge to a state deviating from M_0, a saturation value denoted as M_0^*, with a shorter effective T1 denoted as $T1^*$. The shorter $T1^*$ leads M_z to approach an M_0^* that is less than M_0 [14]. $T1^*$ can be expressed as

$$T_1^* = \left[\frac{1}{T_1} - \frac{\ln(\cos(\alpha))}{TR}\right]^{-1}, \qquad (*)$$

and M_0* as

$$M_0^* = M_0 \frac{1 - e^{-\frac{TR}{T_1}}}{1 - e^{-\frac{TR}{T_1^*}}}. \qquad (**)$$

Where in the case $\alpha \to 0, T_1^* \to T_1$ and $M_0^* \to M_0$ [15].

At the end of the cycle ($MPRAGE_{TR}$), when followed by an inversion pulse, the relaxation will begin from a different start point than in the previous sequence cycle. Consequently, such effect might result in inaccurate signal values. Aiming to avoid this, the term $M_z(end\ of\ cycle)$ in Eq. (8) is necessary. Since it can be utilized in iterating through multiple cycles to ultimately obtain what so called dynamic steady-state/partial saturation of M_z (M_{ss}). This is later of importance to warrant the accuracy of the look-up tables.

The simulation is not restricted to only simulating the MP2RAGE sequence, but also able to simulate up to MPXRAGE (MP3RAGE, MP4RAGE, etc.) by concatenating the above Eqs. (7-10). An additional advantage of the simulation is to investigate the influence of certain factors such as the inhomogeneity of the B_1^+ field and an imperfect inversion ($f_{inv} < 1$) on the MP2RAGE signal and the T1-values estimation.

The standard approach to calculate the look-up Tables, is simply using the nominal readout flip angles (FA) $\alpha_{1,2}^o$ as the MP2RAGE intensity is assumed to be insensitive to variations in B_1^+ [3]. Nonetheless, if the MP2RAGE intensity happens to be susceptible to the inhomogeneity of B_1^+, a modification given by Eq.(11) is required to be implemented in Eq.(9).

$$\alpha_i^o = \alpha_{nominal_i}^o \cdot B_1^+. \qquad (11)$$

Where B_1^+ is considered a factor ranging from 0.4 to 1.4 (40 % - 140 % of the nominal flip angle) to study the influence of the flip angle inhomogeneity and not as the strength of the emitted RF field with the unit Tesla.

2.6.2 From the M_z cycle to MP2RAGE signal

By simulating the magnitude of M_z at every step of the sequence it becomes feasible to determine the MP2RAGE signal at any point. To go from M_z (at the middle of a RAGE train) to the corresponding signal, Eq.(12) can be used. Additionally, Eq.(11) can be implemented in Eq.(12) to simulate the influence of B_1^+ on the signal.

$$S_i = M_i \cdot \sin(\alpha_i^o). \tag{12}$$

Here, i is the first/second RAGE train, S_i is the signal associated with M_i and the $sin(\alpha_i^o)$ term reflects the fraction of M_i that will be projected onto the *xy*-plane (transversal plane).

By picking out S_1 (from the first RAGE train), and S_2 (from the second RAGE train), the MP2RAGE signal can be computed according to Eq.(13),

$$S_{MP2RAGE_{sim}} = \frac{\left(\frac{S_1}{S_2}\right)}{\left(\frac{S_1}{S_2}\right)^2 + 1}, \tag{13}$$

where $S_{MP2RAGE_{sim}}$ represents the MP2RAGE signal computed from the simulation.

As observed, Eq. (13) appears very similar to the left-hand side of Eq. (5). As it can be utilized when dealing with simulations free of noise and arbitrary phase. However, Eq. (13) is rewritten in a different form as it is more convenient for us to work with. The ± sign of S_i will be known in the simulation.

As an outcome of the above, the influence of varying B_1^+ and f_{inv} on the MP2RAGE signal becomes possible to visualize by plotting the MP2RAGE signal versus the different B_1^+-values for a certain assigned f_{inv}.

2.8 Flip Angles and Inversion Efficiency

As mentioned before, there are some challenges associated with the use of UHF scanners that impact the image intensity, such as the bias of the B_1^+ field, and decreased inversion efficiency (f_{inv}) of the net longitudinal magnetization vector, M_z. The inhomogeneity of the B_1^+ field may produce a rather large variation in the local FA, typically 40 % -140 % (smaller and larger values are occasionally observed) of the nominal FA across the brain [5]. Leading to a wide spread of the intensity values in the same kind of tissue. This partly persists even in the MP2RAGE images. Consequently, inaccurate T1-maps and poor tissue segmentation may arise. For that reason, acquiring B_1^+-maps is of importance in our case to enable correction of the look-up table and thus the T1-values. Furthermore, improperly assigned f_{inv} typically 80% - 100% may influence the T1 estimation. Since M_z is only partially inverted, the T1 relaxation occurs earlier in the tissue in comparison with fully inverted M_z.

Therefore, local FA-maps and an adjustment of the f_{inv} factor are required to obtain accurate T1-values and reach reasonable conclusions regarding the anatomical and pathological nature of the tissue.

2.9 K-means vs Histogram Thresholding Segmentation

Segmentation methods such as k-means and histogram thresholding can be exploited as a tool to partition the MP2RAGE brain image into different classes, WM, GM, and CSF (if needed).

As it may appear redundant to utilize two different segmentation methods, it is not completely trivial to know which of these methods will be the most efficient for segmenting WM and GM. Or if there are challenges when dealing with these methods that force the user to compromise between accuracy and time of acquiring the segmentations. The advantage of K-means is that it can automatically find the threshold values based on the number of tissues given as input (*k*-value). While for the histogram thresholding method, its advantage is being very simple to implement. Disadvantages of k-means can be the need to select *k* manually and being dependent on the initial values of the centroids. Disadvantages of histogram thresholding is being time consuming to find the optimal threshold as the peaks in the histogram are not always guaranteed to be narrow or easy to find.

2.9.1 K-means

The k-means clustering is an unsupervised machine learning approach to segment images into a given number of groups, *k*, based on shared properties between the data points using an iterative algorithm. The unsupervised characteristic of k-means enables it to automatically find these shared properties unbiased by the knowledge of the external observer. By rather following simple steps as described below and presented in Fig.6. The only requirement for the method to work is a dataset (images are presented as pixel intensity arrays) and the number of clusters it is to be divided into (*k*) [22].

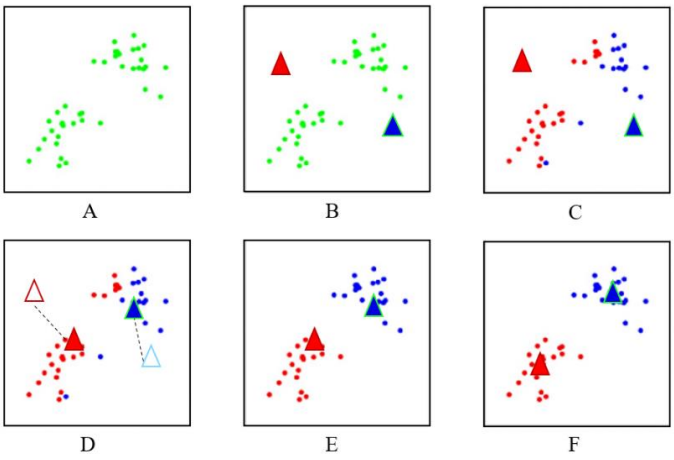

Fig. 6. The process taken by the k-means algorithm to approach k-clusters (k = 2 : red and blue) given a dataset (green). The algorithm picks k-centroids (labels, presented as colored triangles) and position them randomly to later be moved depending on the mean value of the closest cluster. And assign the cluster to the color of the centroid.

The k-means algorithm can be explained by simple steps (shown in Fig.6) being:

1. Input of the dataset into the algorithm.

2. Selected *k*-centroids as an initial suitable guess (in this case $k = 2$) to segment the data into *k*-clusters.

3. By measuring the least-square distance between each point of the dataset to the placed centroids, the location of the closest points to each centroid becomes known enabling labelling them according to the centroid's label (color). As observed, the coloring of the data point depends on the proximity to the centroid.

4. The location of the centroids needs to be updated. The new location is estimated by comparing the mean of the datapoints labelled according to the centroid's label.

5. Step C) is repeated

6. Step D) is repeated

By repeating/iterating through steps C) and D) the algorithm converges to the desired number of clusters and no further centroid movement is required.

Nonetheless, there are poorly separated datasets that might potentially lead to unideal clustering. To avoid that, the algorithm estimates the sum of variance of the labelled data points for each cluster and seeks to recalculate the updated positions of the clusters by placing them randomly aiming to converge to the most optimal clustering [23]. Through minimizing the sum of squares (i.e. variance) according to the expression,

$$\arg min \sum_{i=1}^{k} \sum_{x \in S_i} ||x - \mu_i||^2 = \arg min \sum_{i=1}^{k} |S_i| \, Var(S_i) \quad (14)$$

where **x** is a set of datapoints, $\boldsymbol{\mu_i}$ is the mean value of datapoints within the set S_i, and $Var(S_i)$ is the variance of datapoints within the set/cluster. The variation within each cluster is added to assess the clustering quality.

The selection of the best k is often done manually based on a prior knowledge or educated guess of the number of groups. For example, a suitable initial guess of k for brain images is 3 (WM, GM, and CSF). Still, there are certain techniques relying on analyzing the reduction of variance with increased k, returning the least k-value that contributed to the least reduction of the variance. As a further increase of k will not be valuable.

By default, the algorithm does not require any additional input or adjustments to initiate the segmentation process. Nonetheless, to improve its functionality even further, certain parameters can be customized. These parameters are the criteria, attempts, and the flags. The criteria inform the algorithm to stop iterating when a given criteria is satisfied. A criterion could be the maximum number of iterations (maxITER), an accuracy threshold value (epsilon), or both. As for the attempts, it represents the number of times the algorithm is applied using different labelling in which it will return the labels yielding the most suitable compactness (distance between the datapoints and the centroids). The flags parameter, specifies how the initial centroid positions are placed, being either random or based on a k-means++ method [24].

2.9.2 Histogram Thresholding

The histogram threshold segmentation method is regarded as one of the simplest approaches to partition an image into different classes depending on the pixel intensity range. Let the pixel intensity, $\boldsymbol{I}_{i,j}$ in a 2D image at positions *i* and *j* be given. To achieve segmentation of all the pixels with value $\boldsymbol{T}$ and higher, the

remaining pixels with $I < T$ are assigned to 0. To create a binary mask of the remaining pixels, their values are assigned to 1. The value of T is referred to as the threshold value.

By utilizing the multiplication of the mask with the original image, a segmented part of the image can be obtained. To find a suitable threshold value (T), an image intensity histogram is plotted. An illustration of an MP2RAGE brain image histogram is shown in Fig.7.

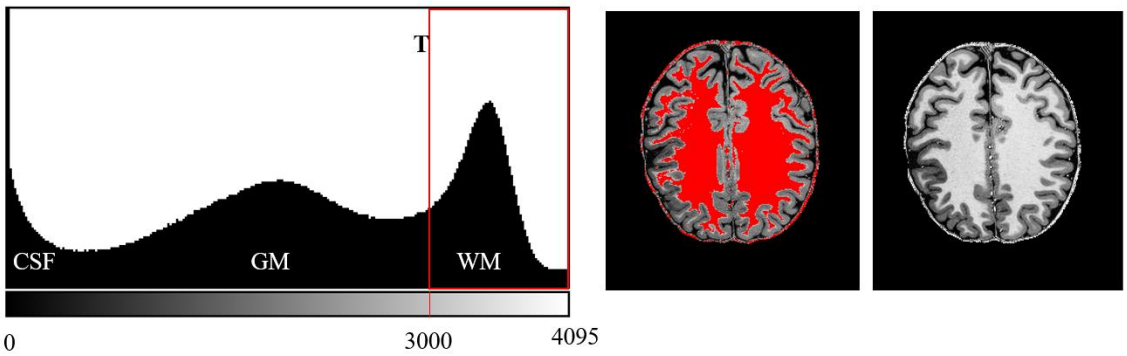

Fig. 7. Left**;** Histogram of an MP2RAGE brain image slice showing three peaks identified as WM, GM, and CSF. Right; the potential location of the pixels intensities above the threshold value (T = 3000 ms) responsible for representing white matter (WM) are highlighted in red. In this illustration, the intensity of the MP2RAGE image is scaled to [0, 4095] instead of [-0.5, 0.5].

2.10 Adiabatic inversion pulses

The adiabatic pulses belong to a class of RF pulses that are both amplitude -and frequency-modulated. These pulses tend to be partially insensitive to the inhomogeneity of the B_1 field and B_0 variations in the MRI scanner [25]. This property empowers the adiabatic pulses to become less sensitive to B_1 field inhomogeneities than traditional RF pulses, maintain spin control over wide range of B_1^+ and RF power levels (from the RF amplifier), and reduce the specific absorption rate (SAR) [26]. However, the pulses require a rather long pulse duration (width) or a relatively high B_1 amplitude to satisfy the *adiabatic condition*. This condition implies that in order to achieve an efficient inversion of M_z, the rate of change in the direction of the effective B_1-field ($\mathbf{B_{1eff}}$) should be much slower than the magnitude of B_{1eff}. Mathematically, this condition is formulated as

$$\left|\frac{d\phi}{dt}\right| \ll \gamma \left|B_{1eff}\right| \qquad (15)$$

where the ratio $\frac{d\phi}{dt}$ represents the angular frequency.

To control the peak amplitude of the "Full adiabatic" pulse inversion, a nominal value defined as *B_1-max* is altered in the scanner's user interface. If the amplitude happens to exceed a certain threshold B_1-value, M_z becomes less susceptible to the inhomogeneity of the B_1 field in the scanner. Hence, a more spatially homogenous inversion of M_z takes place [25].

Furthermore, the designing of adiabatic pulses is not a trivial task as they are often derived from hyperbolic tangent/secant functions to later independently and simultaneously model their amplitude and frequency [27]. There are several adiabatic pulses that are currently used within MRI, an example of these are the "Full adiabatic" pulse and the frequency offset corrected inversion (FOCI) pulse [26].

3 Material and Methods

3.1 Simulations

The simulations of specific MP2RAGE protocols [28] are conducted in Python (version 3.8) to investigate the influence of B_1^+ and f_{inv} on M_z, the MP2RAGE signal, and estimated T1. All the simulations below are conducted using Eqs.(7-13) and based on the sequence parameters in Table 1. The created code is provided on GitHub [29]. Simulations of the M_z-dynamic and MP2RAGE signals for WM, GM and CSF are conducted. The T1-values used for either medium are 1200 ms, 1800 ms, and 4000 ms respectively based on literature [2].The selected range for B_1^+ is [40%,140%] and for f_{inv} it is [80%,100%].

3.1.1 Simulation parameters

In order to start simulating an MP2RAGE sequence, certain parameters are required to be known. These parameters are (note that M_0 and T2* cancel out in MP2RAGE, hence, they are not included):

- The flip angles α_1^o / α_2^o.
- The length of the cycle $MP2RAGE_{TR}$.
- The encoding steps RL TurboFactor (Philips)/Slices per slab (Siemens).
- The TR (Philips)/Echo spacing (Siemens).
- The length of the RAGE train (TurboFactor; on Siemens identical to RL encoding).
- The TI_1 / TI_2 values.
- The location of central k-space line readout (beginning/middle of the RAGE train).

Parameters requiring an initial guess for the simulation:

- The T1-value of the tissue.
- The assigned value for B_1^+.
- The assigned value for the inversion efficiency factor (f_{inv}).

The value of the above parameters used in the simulation can be seen in Table 1 [28].

Table 1. Assigned values of the simulation parameters to simulate the M_z relaxation during a specific MP2RAGE protocol [28].

Parameter	Unit	Value
T1-values: WM/GM/CSF	[ms]	1200/1800/4000
Flip angles: α_1^o / α_2^o	[degrees]	$5^o / 3^o$
$MP2RAGE_{TR}$	[ms]	5000
Encoding steps RL		257
TR	[ms]	6.8
TurboFactor/Echo TrainLength		256
Duration of RAGE	[ms]	1741

TI_1/TI_2	[ms]	900/2750
Central k-space readout		Middle of RAGE
Assigned B_1^+	[%]	100
Assigned f_{inv}	[%]	96

3.1.2 B_1^+ influenced longitudinal magnetization relaxation

To consider the potential influence of the inhomogeneous B_1^+ field on the simulated M_z relaxation in MP2RAGE, Eq.(9) is utilized to replace the nominal flip angles by the local flip angles α_1^o/α_2^o . This is done by assigning B_1^+-values varying from 40% up to 140% in the simulation. The B_1^+-maps are obtained through a DREAM sequence protocol with STEAM flip angles equal to 25°, 40°, 60°, and 90°.

3.1.3 Inversion efficiency factor influenced relaxation

The variations in the inversion efficiency factor, f_{inv}, may lead to different starting points post inversion of M_z. To investigate this, different assigned values of f_{inv}, ranging from 80% to 100%, are simulated.

3.2 Experiments

Healthy adult subjects were scanned on an actively shielded 7T MR system (Achieva, Philips Healthcare, Best, NL) at the Swedish National 7T Facility, Lund University Bioimaging Centre, LU. An RF head-coil using a dual-transmit head coil with a 32-channel receive array was used (Nova Medical, Wilmington, MA). Informed written consent was obtained prior to each examination as supervised by the Swedish ethics review authority.

1. Typical measurement protocol: Provided in subsection 3.4.
2. Typical MP2RAGE sequence: Provided in Table 1 [28].

Two dedicated experiments were performed to investigate specific behavior of the MP2RAGE sequence.

3.2.1 Experiment 1

For subjects with large head sizes, the 2x4kW peak power provided by the two RF amplifiers (CPC, Hauppauge, NY) may not be enough to create the maximum specified B_1 of 20 µT. Thus, the B_1-max needs to be reduced to 18 µT or even 15 µT. To study the influence of B_1-max, a male subject (30 years) was scanned using the "Full adiabatic" inversion pulse at different B_1-max =15µT, 12µT, 9µT, 6µT. (18µT were precluded by head size). The nominal flip angle kept constant at 1800°, leading to a variation of the pulse duration.

3.2.2 Experiment 2

To mimic a variation of B_1^+ through alteration of B_1-max, the pulse duration needs to be kept constant during the experiment. The simulated change of B_1^+ allows us to have a constant location of the ROIs for different B_1-max images. In another volunteer, (male, 26 years)

B_1-max and nominal flip angles were varied in parallel through 20µT, 18µT, 15µT, 12µT, 9µT, 6µT, 3µT and 2000°, 1800°, 1500°, 1200°, 900°, 600°, 300°, respectively.

In addition, a novel FOCI inversion (2250°) was compared to the default "Full adiabatic" (1800°, 12µT).

An in-house software modification made it possible to apply a higher FA in the second RAGE train relative the first. This should reduce the sensitivity to B_1^+ inhomogeneity [3].

3.3 Simulation-based adjustment of the inversion efficiency factor

Given that the MP2RAGE images can be obtained through Eq. (5), the B_1^+-maps are then combined and co-registered to the PDw part of the MP2RAGE images using the FSL library tool, FLIRT [30][31]. Next, the skull stripped MP2RAGE images (the skull stripping method is explained in detail in subsection 3.5) are overlaid with the skull stripped B_1-map to obtain what is illustrated in Fig.8. The following enables ROI selection of certain regions in the brain/tissue to obtain both the image intensity-and the B_1^+-value from the same ROI. The acquired values are later plotted and compared to the predicted output from the simulation for different f_{inv} (for a specific T1-value). By plotting the obtained experimental data from the test subject versus the output from the simulation, a suitable f_{inv} might be found for the 7T Philips MRI scanner (assuming that the chosen T1-values in the simulation are reasonable enough for respective tissues).

The simulation is conducted for both WM and GM for different f_{inv}.

Fig. 8. Illustration of the overlaying (C) of a skull stripped MP2RAGE image (A) and a B_1^+ local flip angle map (B) obtained from multiple DREAM measurements. In C) co-registration enables a readout of the MP2RAGE signal intensity and its corresponding B_1^+-value for each pixel.

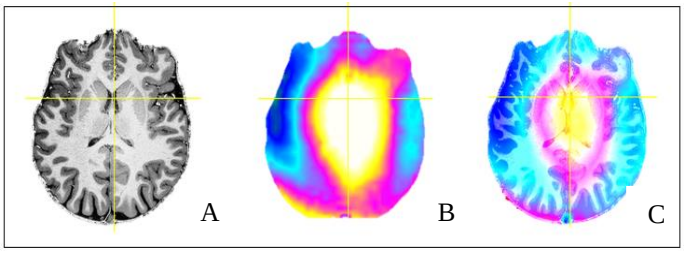

3.4 MP2RAGE measurements on the 7T Philips scanner

To obtain the MP2RAGE images and the B_1^+-maps using the 7T Philips scanner, the steps below are followed.

- Coil survey scan 32-channel receive array transmitter: check of the functionality of the coil channels.
- Survey
- B_0-map (unshimmed)
- B_0-map shimming: utilizing a semi-manual shimming tool to obtain shimming parameters.
- SENSE reference scan
- MP2RAGE sequence: to obtain the MP2RAGE image volumes.
- Delayed reconstruction of real and imaginary signal
- 4xDREAM sequences

3.5 Data-processing and Segmentation

The magnitude, real and imaginary 2D DICOM files (*int16*) were transferred from the scanner to a server to be converted into 3D NIfTI volumes, restoring signal scaling in arbitrary units. From the latter, 3D MP2RAGE images (float) were calculated. An illustration of a calculated MP2RAGE image is presented in Fig.4. The calculated MP2RAGE images require some pre-processing to become friendlier to work with, due to unwanted noise in certain areas of the brain images. Additionally, some segmentation tools are optimized to be applied to *int36* or *int16* image data format, while others require an *int8* format. These tools are yet to be modified to be deployed on NIfTI (commonly used within neuroscience) format MR images. Another common MR image format is DICOM. However, all images obtained from the 7T Philips scanner are converted to a NIfTI format.

3.5.1 Brain extraction

To obtain decent whole brain histograms of the MP2RAGE images (reduce noise), an FSL library is exploited [31]. First, we seek the extraction of the brain from the noisy MP2RAGE images, to later be used in our research. This was conducted by utilizing the Brain Extraction Tool (BET) [32], and used on the PD-weighted (PDw/S_{TI_2}) image from MP2RAGE. Since, the brain tissue in the PDw images appear uniformly bright across different tissue types (in comparison to the T1-weighted (T1w) images) and contain less noise than the MP2RAGE images. The GM appear darker in the T1w images making BET more susceptible to misinterpreting the tissue as the edge of the brain. Utilizing the brain extraction on the PDw images, a mask of the brain is obtained and applied to the MP2RAGE images. Thus, a clearer and less noisy brain extraction is acquired. This process is shown in Fig.9.

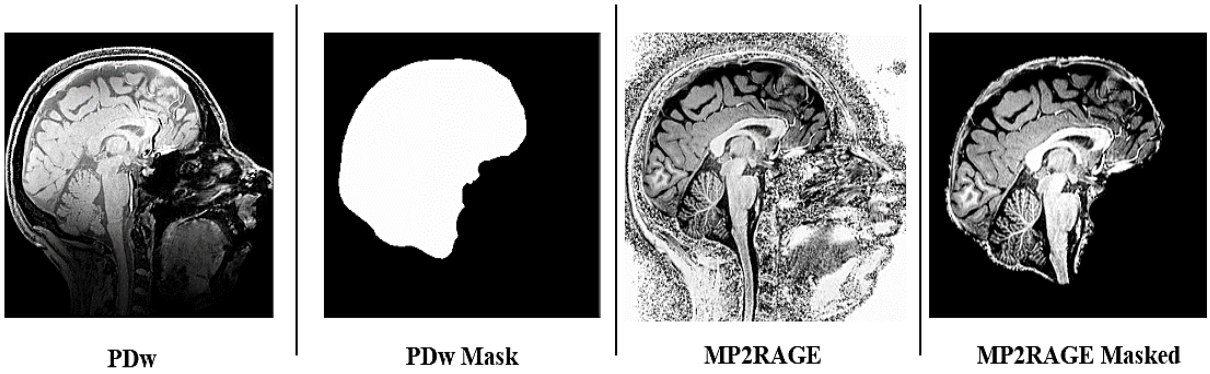

Fig. 9. An illustration of the brain extraction process to obtain skull surface stripped MP2RAGE brain images. Brain extraction (BET) is performed on the proton density weighted (PDw/S_{TI_2}) image to obtain a mask which is then applied to the MP2RAGE image.

3.5.2 K-means and histogram threshold segmentation

To facilitate the visualization of tissues and to assess the impact of B_1^+ and f_{inv} on the T1 estimation in WM and GM, segmentation methods such as k-means and histogram thresholding are exploited. For these methods to be reliable, an absence of "spatial bias" occurring due to variation of B_1^+ is required; as they assume a consistent T1. As presented in Fig.8, overlaying of the B_1^+-map and the MP2RAGE image results in several distracting tissue details when we are interested in picking ROI values for a specific tissue (WM or GM). To simplify the process, segmentation methods such as k-means and histogram thresholding are compared and applied to the images. More on this can be found in section 8.

3.5.2.1 K-means

To implement the k-means algorithm on the NIfTI formatted MP2RAGE images in Python, the images are required to be converted to a *float*32 PNG format. Later, a properly selected *k* is chosen. The parameter values selected are the following:

1. *Criteria:* chosen to be both maxITER and epsilon and set to 10 and 1.0 respectively.
2. *Attempts*: number of attempts is set to 10
3. *Flags*: KMEANS_RANDOM_CENTERS

The outputs of the algorithm are the compactness of the clusters, labels of the clusters (red, blue, etc.), and the centers of the found clusters.

3.5.2.2 Histogram threshold

The histogram threshold segmentation method can be implemented on the MP2RAGE images by selecting a suitable threshold value, *T* and segment out all the pixel values above that *T* limit. To find *T* for the segmentation of the WM and GM tissues, a histogram over the MP2RAGE pixel intensity is created. The selection of *T* is done manually by varying the threshold until an acceptable segmentation is achieved.

3.6 T1-mapping

3.6.1 T1-mapping and a B_1^+ map

To create a T1-map based on the MP2RAGE image intensity, an already provided script by J. P. Marques et al [3] in MATLAB is utilized [33]. The f_{inv} value in the code is set to 0.96 (96% inversion efficiency) by default.

The script generate the T1-maps based on the input of the MP2RAGE sequence parameters (TI_1/ TI_2, TR, $MP2RAGE_{TR}$, α^o_1/ α^o_2, slices per slab, and f_{inv}) and the B_1^+-map variation. The script creates an MP2RAGE intensity and T1 lookup Table (LUT) for the flip angles. Thus, by reading the MP2RAGE pixel intensity together with its corresponding B_1^+-value, the associated unique T1-value may be acquired from the LUT. By creating a broad set of simulated values, linear interpolation can be utilized to obtain a T1-value for the given MP2RAGE and B_1^+. The signal range must be between [-0.5, 0.5] while the T1-values are set to be between [500 ms, 5000 ms] in the code.

As an output, the code returns an image volume where each pixel intensity is replaced by its corresponding T1-value, as illustrated in Fig.5.

If a co-registered B_1^+-map is provided, the code returns T1-values based on the local readout flip angles.

3.6.2 T1-mapping and the inversion efficiency factor

To study the influence of assigning different f_{inv} on the accuracy of the T1-values, a selected range of f_{inv} -values; 0.80, 0.84, 0.88, 0.92, 0.96, and 1.0 are substituted in the code. The variation in the T1-values for each assigned f_{inv} can then be compared to the expected value in a specific ROI in both WM and GM.

3.6.3 T1-mapping and the selection of pulse type and amplitude

A comparison between the "Full adiabatic" and the FOCI pulses are performed to evaluate their impact on the MP2RAGE images. Three protocols are implemented with variation in the pulse types, nominal flip angles α_1^o/α_2^o , $f_{inv,}$ and B_1-max, as presented below in Table 2.

Table 2. Used parameters of the adiabatic pulses to estimate their impact on the T1-maps.

Pulse type	α_1^o	α_2^o	***B1-max*** [µT]			f_{inv} [%]						
Full adiabatic	5°	3°	6	9	12	80	84	88	92	94	96	100
FOCI 53	5°	3°	12			80	84	88	92	94	96	100
FOCI 45	4°	5°	12			80	84	88	92	94	96	100

Next, the obtained T1-volumes are examined by utilizing ROI selection of specific regions of the brain to assess any variations in the T1-values.

3.6.4 Validation of method

For every newly created model or simulation, a validation process is required to increase the reliability of the achieved results. As a validation, a previously published MP2RAGE protocol outcome by J. P. Marques et al [3] is compared to the output of our simulation. The published MP2RAGE protocol parameters are implemented in the simulation to obtain T1. If the obtained T1 values are identical to the T1 values published by Marques's MATLAB code, the simulation is considered valid enough to be exploited for further protocols simulations. An additional protocol that is exploited for comparison is published by R. A. M. Haast et al [34] (*Maastricht*).

The simulation begins by implementing the protocol parameters and simulating the behavior of M_z and the MP2RAGE signal for a set of T1-values [500, 4000] where each new T1-value is simulated for different set of B_1^+ (40% - 140%) and an $f_{inv} = 0.96$.

To validate the simulation experimentally, the MP2RAGE protocols given in Table 2 are used in an experiment where the outcome will later be compared to the simulation outcome of the same protocols. Some examples of the simulation outcomes may be predicting the prominent variations in contrast, signal intensity or the accuracy of the T1-estimation.

3.7 Influence of head size on the MP2RAGE images and T1-maps

In the 7T head coil, the head size of the subject may play a role in deciding the maximum amplitude of the adiabatic pulse, B_1-max, that can be delivered by the scanner (more spins to invert). Consequently, the inversion efficiency across the brain could be decreased as the scanner constrains the user to a limited range of B_1-max values.

Two test subjects, one with a relatively large and another with a small head size were scanned following the protocol in Table 1. To evaluate the effect on the MP2RAGE image quality, a visual evaluation is made of the T1- (obtained at TI_1) and PD-weighted (obtained at TI_2) images for the different B_1-max values allowed by the scanner. To evaluate the influence on the T1-maps, a selection of ROIs in different regions of the brain in WM and GM for used B_1-max and assigned f_{inv} are utilized.

4 Results

4.1 The B_1^+-map correction and inversion efficiency importance

When forward modeling the T1-maps utilizing the specific MP2RAGE protocol, the option of including the B_1^+-maps is of importance to consider as illustrated in Fig.10. In aim to avoid systematic errors leading to asymmetric and T1-maps and different T1 across the brain. Here, the inversion efficiency (f_{inv}) is set to 0.96 (96 %) as it is the default value in the MATLAB code (by Marques) and commonly found in literature [3] [32]. The majority of the low B1+-values are found around lower regions of the brain (e.g., cerebellum, temporal lobe).

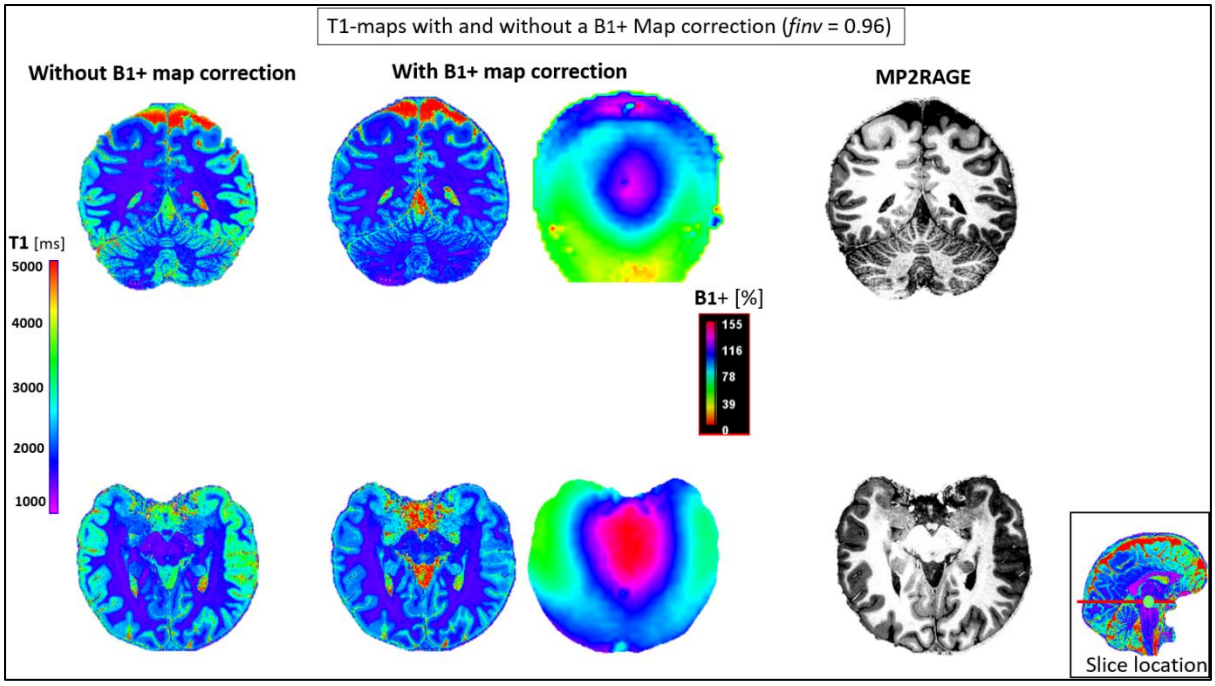

Fig. 10. T1-maps (coronal and axial oriented) with and without the B_1^+ correction for inversion efficiency (*finv*) equivalent to 0.96. The spatial right-left asymmetry correlated to B_1^+ points to systematic error observed in the T1-maps calculated without the B_1^+ correction, in addition to a clear deference in T1 in peripheral low B_1^+ areas.

To assess the influence of the B_1^+ correction on the calculated T1-maps, histograms of the corrected and uncorrected maps are presented in Fig.10 is given in Fig.11. Without the B_1^+ correction, the T1-values were overestimated in addition to observing broader WM-and GM-peaks. Furthermore, a narrower second CSF peak appears in the corrected T1-maps.

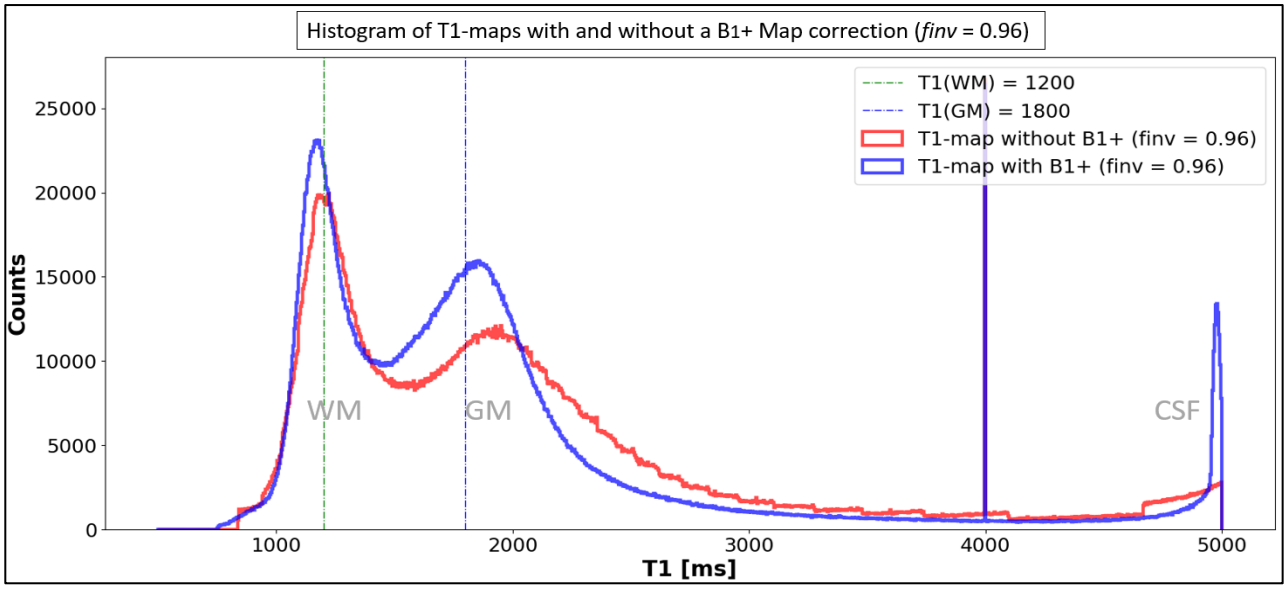

Fig. 11. Histogram of the calculated T1-maps with (blue) and without (red) a B_1^+-map. Overestimation of T1-values in GM and broader WM-and GM-peaks are observed in the uncorrected T1-maps. Additionally, the second CSF peak is wide and flattened in the uncorrected T1-map in comparison to the corrected T1-map. Vertical dashed lines indicate the expected T1-values for WM and GM as in reference [2].

A visualization of the ratio between the corrected and uncorrected T1-maps is computed and presented in Fig.12.

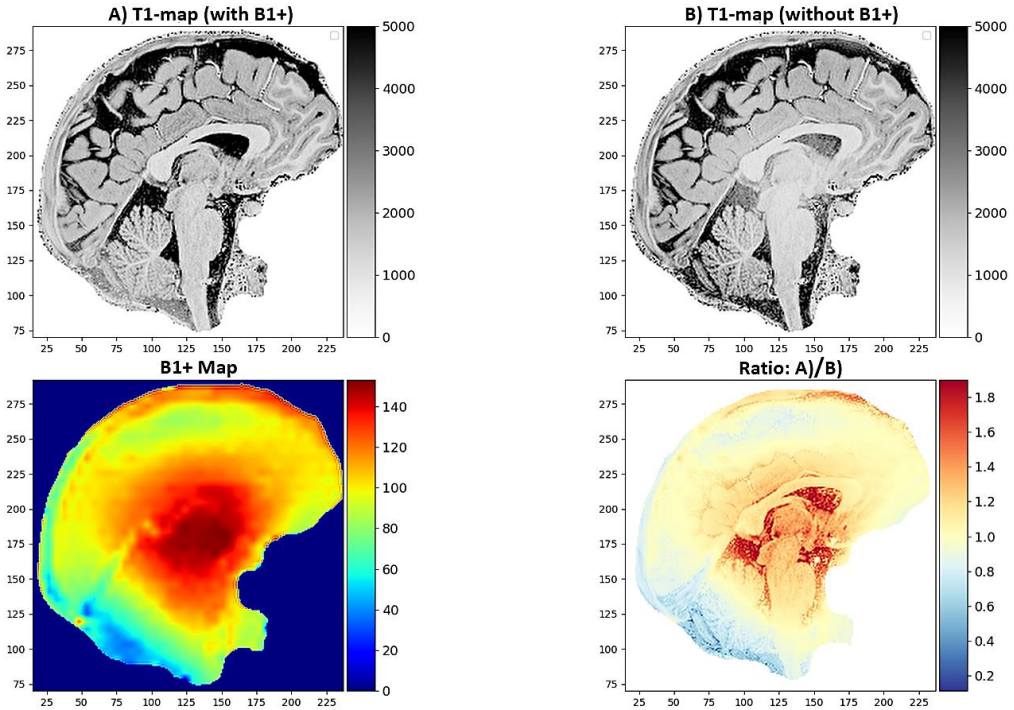

Fig. 12. Sagittal view of corrected and uncorrected T1-maps along with their ratio and corresponding B_1^+-map. Lower T1-values are observed in regions with low B_1^+-values and vice versa.

Based on the results above, all the presented results below will be evaluated with the B_1^+ correction to avoid systematic error. In which continuously, will be referred to as the 'corrected' entity.

The inversion efficiency factor (f_{inv}) is set to 0.96 in Figs.(10-12). Nonetheless, readjusting f_{inv} to 1.0 (100 %) results in lower T1-values as shown in the histogram in Fig.13. Unsurprisingly, all the pixels are affected.

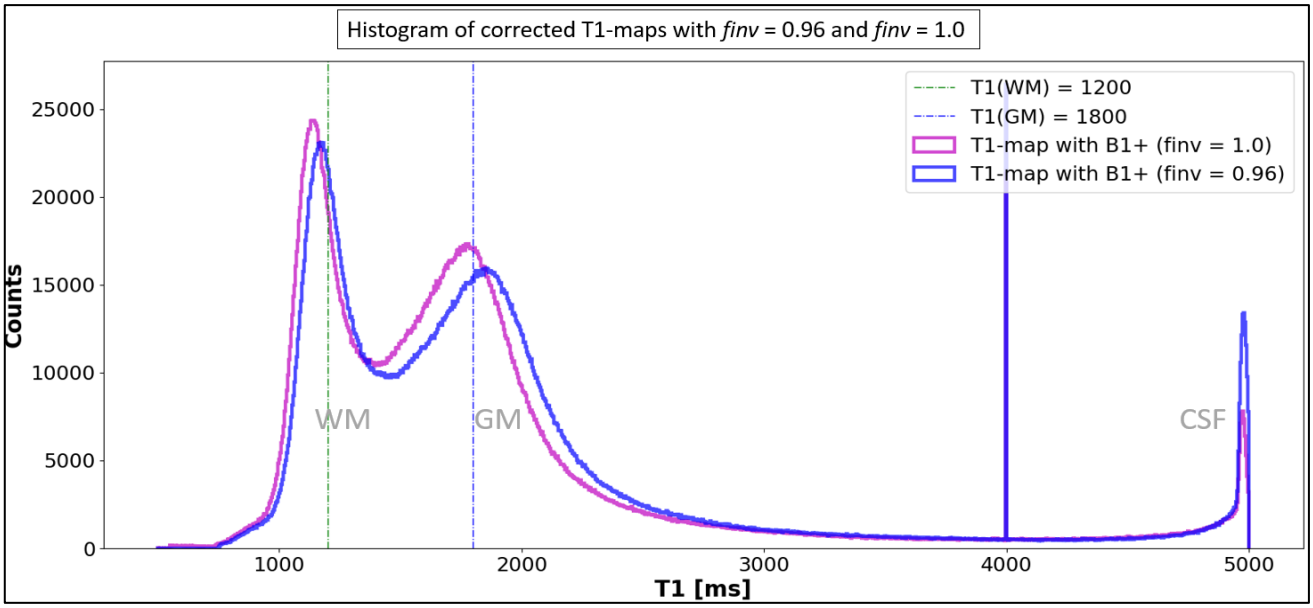

Fig. 13. Histogram of corrected T1-maps with different f_{inv} being 0.96 (96 %) and 1.0 (100%). Lower T1-values for WM are observed in the T1-map with f_{inv} = 1.0 while the GM peak is thinner and closer to the expected T1 value for GM (about 1800 ms) taken from literature [2].

4.2 Simulations

Based on the knowledge from the results in 4.1, simulation procedures are conducted to investigate the influence of B_1^+ and f_{inv} on the calculated T1-maps.

4.2.1 Simulations of M_z and MP2RAGE signal versus B_1^+

To start with, the M_z relaxation during the MP2RAGE sequence is simulated in WM, GM and CSF, for f_{inv} = 0.96 and B_1^+ = 1.0 (100 % of the nominal flip angle) as used in the default LUT and presented in Fig.14. Next, to study the influence of a varying B_1^+ on M_z, assigned B_1^+-values varying from 40% up to 140% are included in the simulation to obtain Fig.15.

Now that M_z is known for the different B_1^+-values, the signal $S_{MP2RAGE}$ can be calculated at each B_1^+ point according to Eq.(13), where S1 and S2 are obtained from Fig.(15). The $S_{MP2RAGE}$ versus the assigned B_1^+ in WM, GM and CSF for f_{inv} = 0.96 are presented in Fig.(16). The MP2RAGE pixel value is increasing with increased B_1^+.

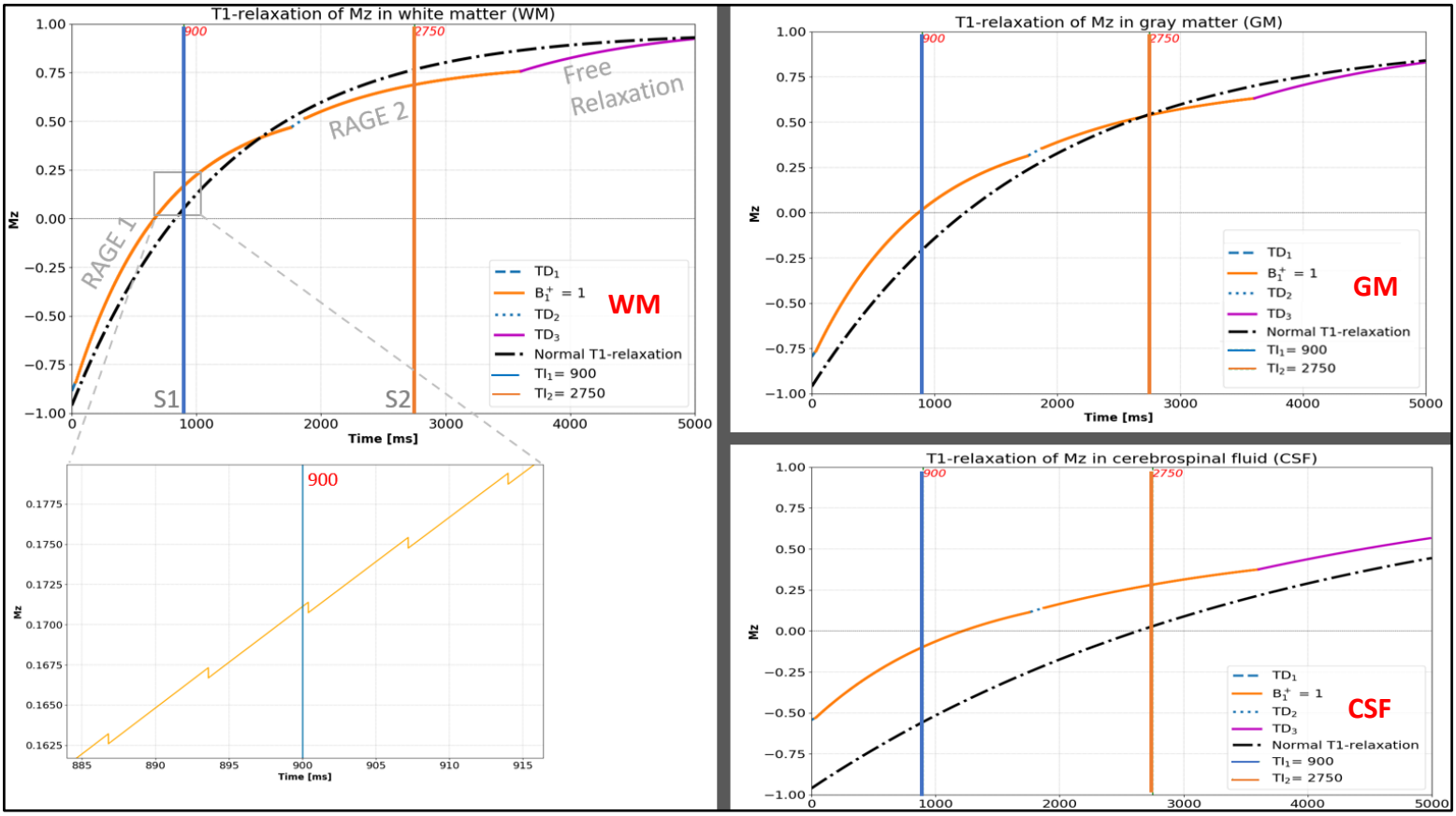

Fig. 14. The M_z relaxation during the MP2RAGE sequence is simulated in WM, GM, and CSF, for f_{inv} = 0.96 and B_1^+ = 1.0 (100 % of the nominal flip angle). The S1 and S2 points at TI_1 and TI_2 highlighted in the figures represents the center of the k-space line in the second-phase encoding direction, where the T1-weighted and the PD-weighted MP2RAGE images are obtained. The selected T1 values according to Table 1 for WM, GM and CSF are 1200 ms, 1800 ms, and 4000 ms, respectively.

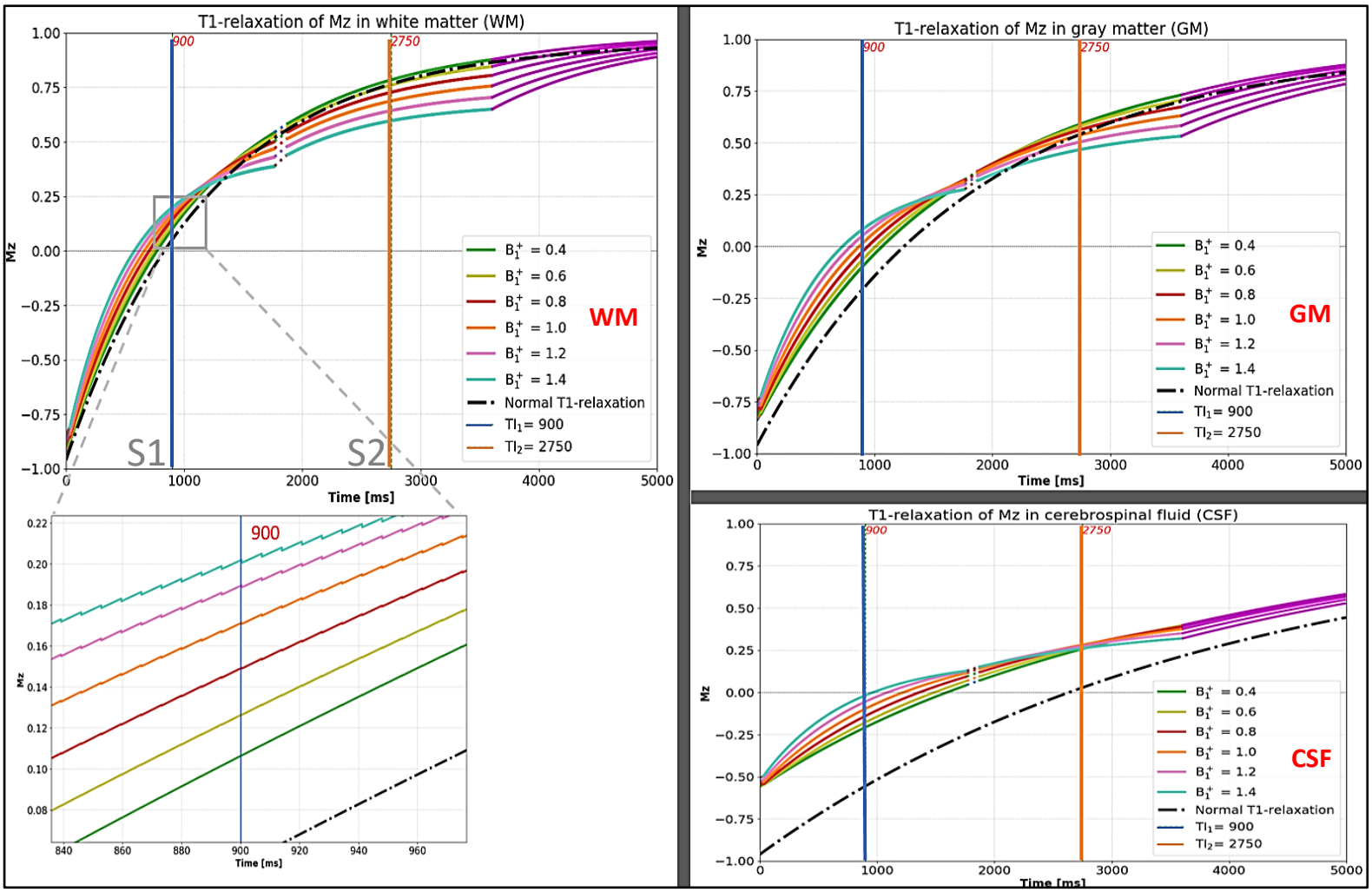

Fig. 15. The M_z relaxation during an MP2RAGE sequence is simulated in WM, GM and CSF, for f_{inv} = 0.96 and a set of assigned B_1^+-values from 0.4 (40 %) up to 1.4 (140 % of the nominal flip angle). The S1 and S2 points at TI_1 and TI_2 are highlighted, from which the MP2RAGE signal, $S_{MP2RAGE}$ is calculated. The T1 values for WM, GM and CSF are 1200 ms, 1800 ms, and 4000 ms respectively (Table 1).

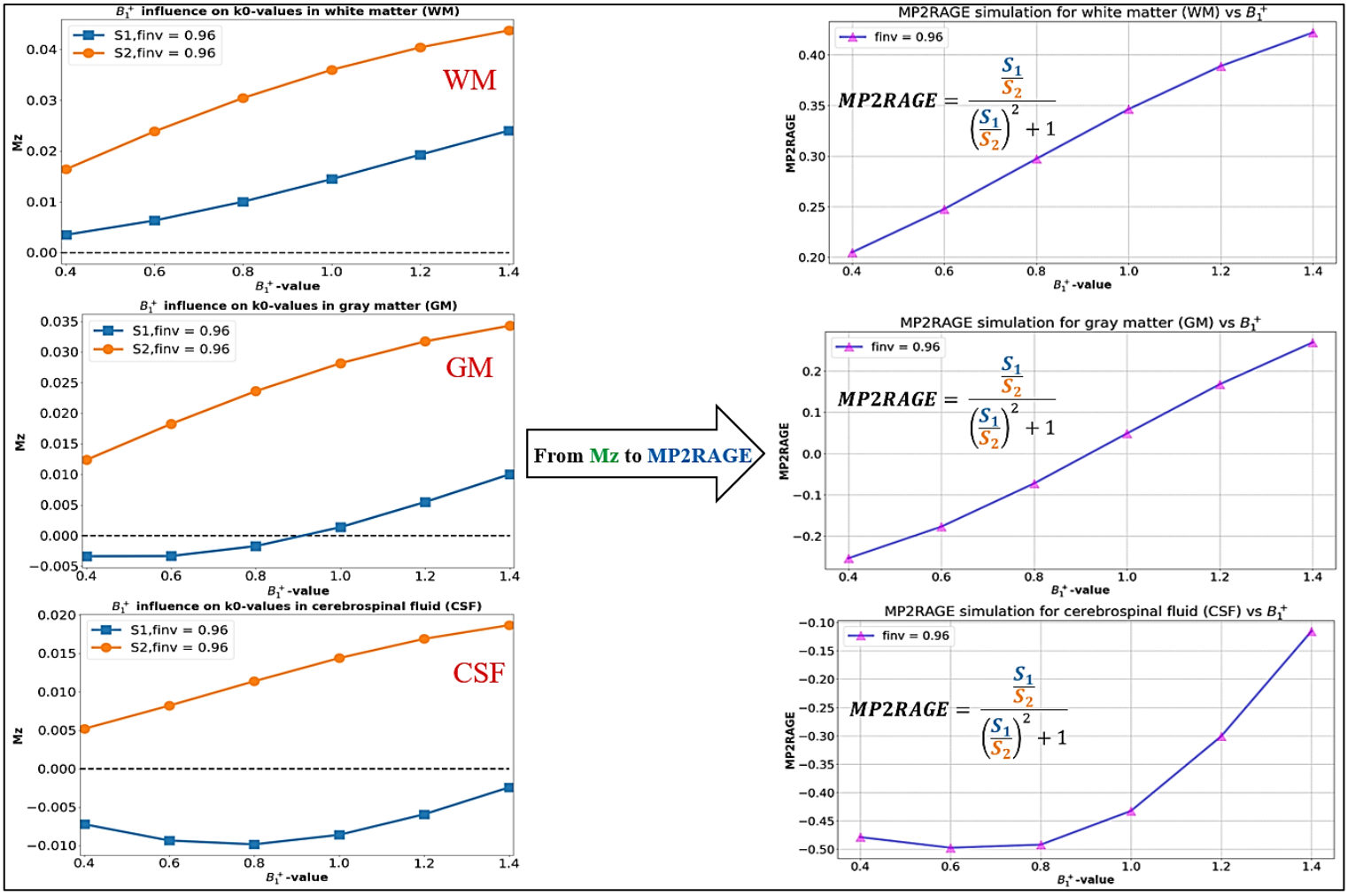

Fig. 16. **Simulation of B_1^+ dependence.** Illustration of transition from the M_z relaxation to the MP2RAGE signal for WM, GM and CSF for f_{inv} = 0.96 and a set of assigned B_1^+-values from 0.4 (40 %) to 1.4 (140 % of the nominal flip angle). The S1 and S2 points calculated using Eq.(12) at TI_1 and TI_2 are substituted in Eq.(13) to calculate $S_{MP2RAGE}$ (referred to as *MP2RAGE* in the figures). The k0-values (left figures title) are the values of S1 and S2 at the center of the k-space line in the second-phase encoding direction

4.2.2 Simulations of MP2RAGE signal versus inversion efficiency

As observed, all the conducted simulations above are made for a specific and constant f_{inv} (0.96). However, depending on the region of the brain, the pulse type, and other protocol parameters (flip angles, $MP2RAGE_{TR}$), the f_{inv} -value can change and influence the MP2RAGE signal. Therefore, we proceed by simulating the effects of a varying f_{inv} on the MP2RAGE signal in Fig.(16).

To simulate the effect of a varying inversion efficiency, a selected range of f_{inv} -values from 0.8 (80 %) up to 1.0 (100 %) are inserted in the simulation according to Eqs. (7-13). The outcome is presented in Fig.(17) for MP2RAGE versus B_1^+ for different assigned f_{inv} in WM, GM and CSF respectively.

In Fig.(17), a deviation in the MP2RAGE values is shown if the inversion efficiency happens to differ from the regularly used value 0.96. The deviations in WM, GM, and CSF at the lowest and highest B_1^+ of f_{inv} =0.96 are: WM (86%, 155%) (97%, 107%), GM (92%, 151%) (95%, 120%) and for CSF (22%, 110%) for B_1^+ = 1.0.

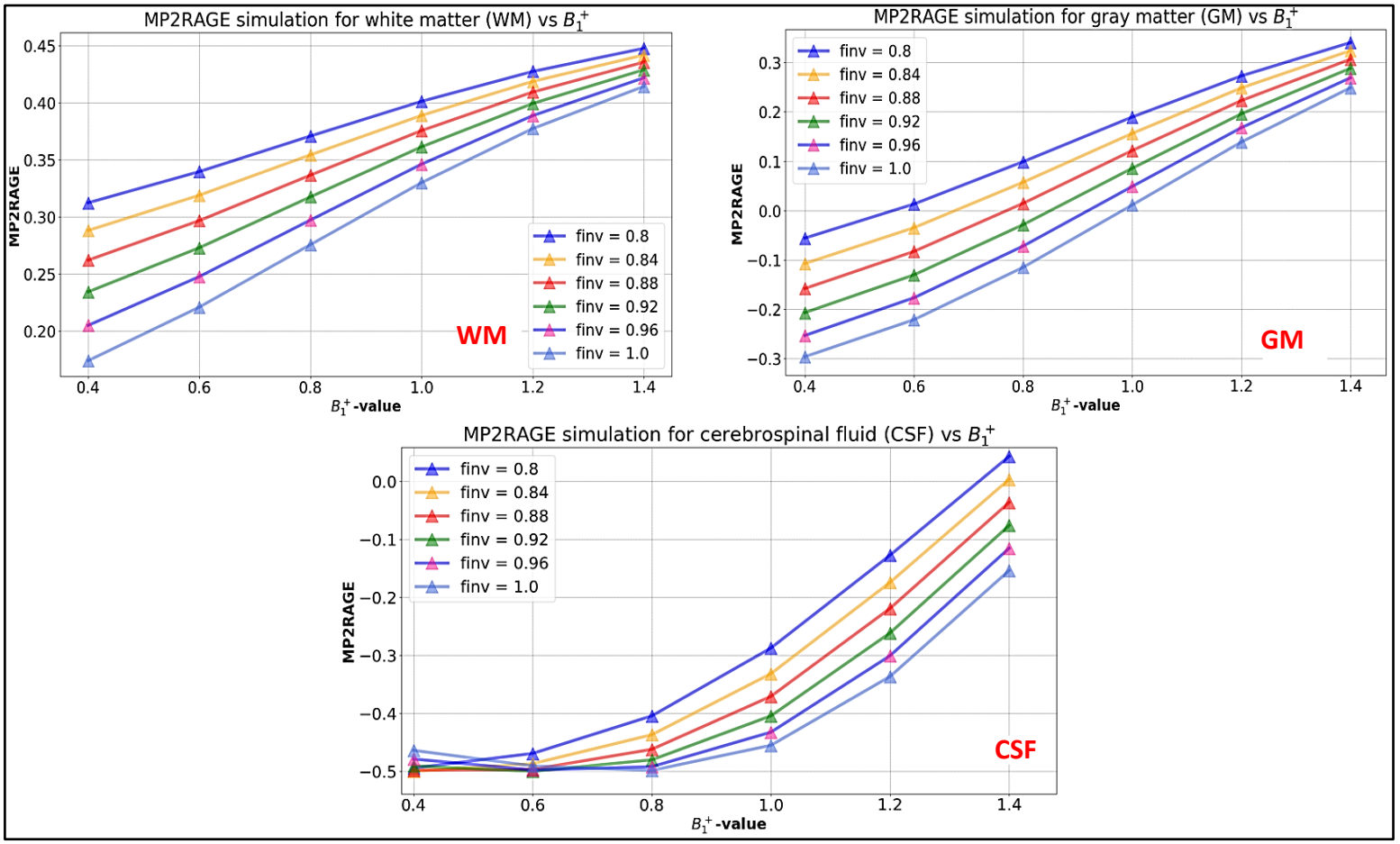

Fig. 17. Simulation of MP2RAGE versus B_1^+ for an assigned range of f_{inv} [0.8 (80%) -1.0 (100%)] in WM, GM, and CSF respectively. For WM and GM, it can be observed that at lower B_1^+-values the variation of f_{inv} leads to a large MP2RAGE disparity in comparison to occurring around high B_1^+-values.

4.3 Estimating a suitable inversion efficiency factor

In aim to find f_{inv} based on the location of the experimentally obtained values in relation to the simulated ones for different f_{inv}, the selected ROIs along with their experimental values in WM and GM are shown in Fig.(18). The data points represent the mean in each ROI. The error bars indicate the standard deviation.

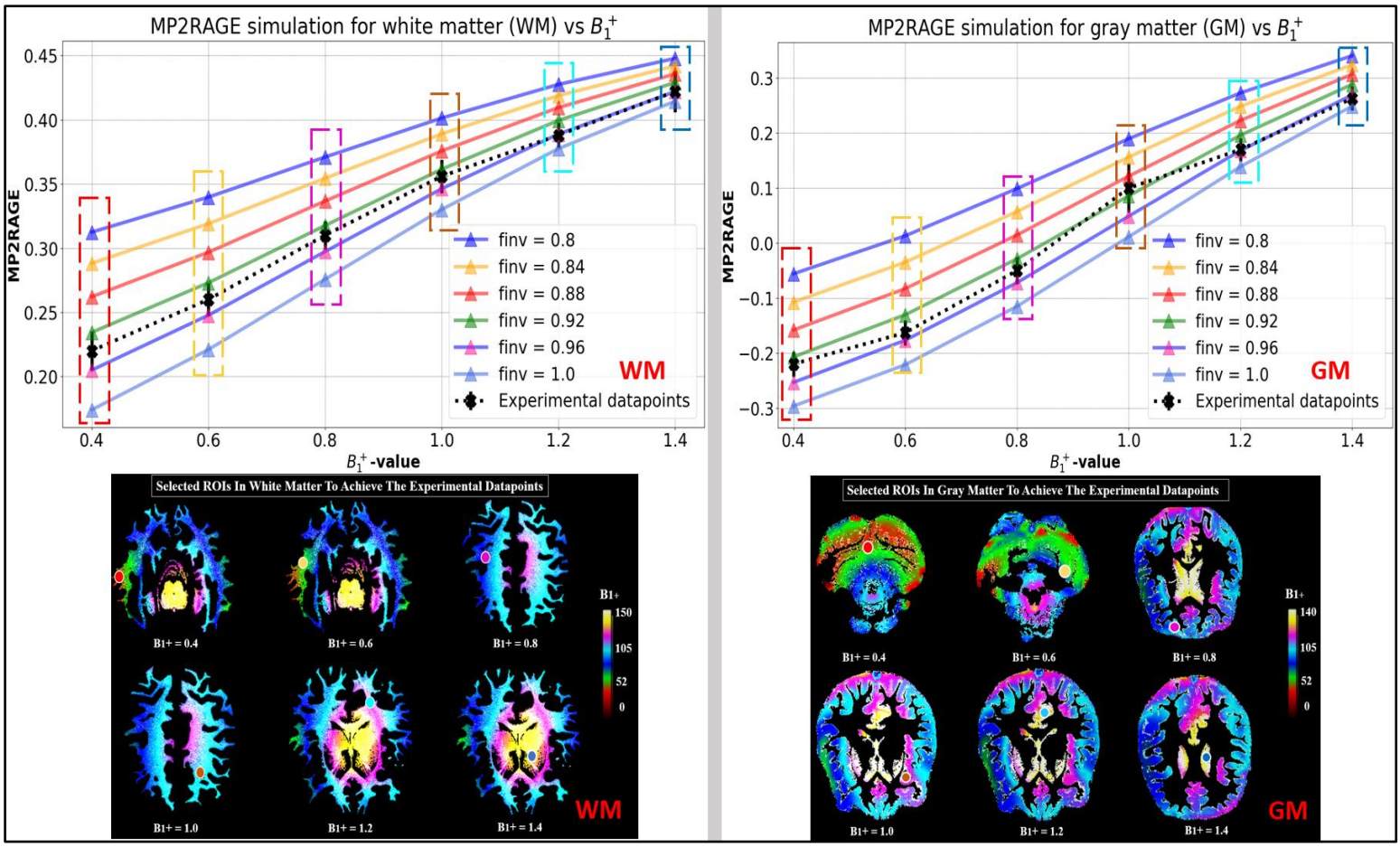

Fig. 18. A comparison of the simulated MP2RAGE versus B_1^+-plots for different f_{inv} with the experimentally obtained datapoints (black, dotted line), indicates a suitable f_{inv} hypothetically leading to more accurate T1-map. The Selected ROIs are shown below together with the color bars indicating B_1^+ at each ROI in WM and GM. The error bars indicate the standard deviation.

From the acquired results in Fig. (18), it is apparent that the correct f_{inv} -value lies in between f_{inv} = 0.92 and 0.96. The f_{inv} -value is a control variable in the T1-maping script [33]. **Hence, a more appropriate value of f_{inv} should be <u>0.94</u> for the standard "Full adiabatic" inversion pulse (1800º, B_1-max= 18 µT).**

Next, we proceed to recalculate the T1-maps with the newly found f_{inv} to investigate the improved/worsened accuracy of the corrected T1-maps through creating a T1 histogram of the images. The histogram is made of the images presented in Fig.(10) to relate it back to the histogram in Fig.(13), as illustrated in Fig.(19). In Fig.(19) it is shown that the f_{inv} = 0.94 value leads to a WM-peak closer to the expected T1 value for WM (1200 ms) while obtaining a GM-peak shifted to higher T1 relative the theoretical GM T1 (1800 ms). Additionally, a higher CSF peak is observed in comparison to the other assigned f_{inv}.

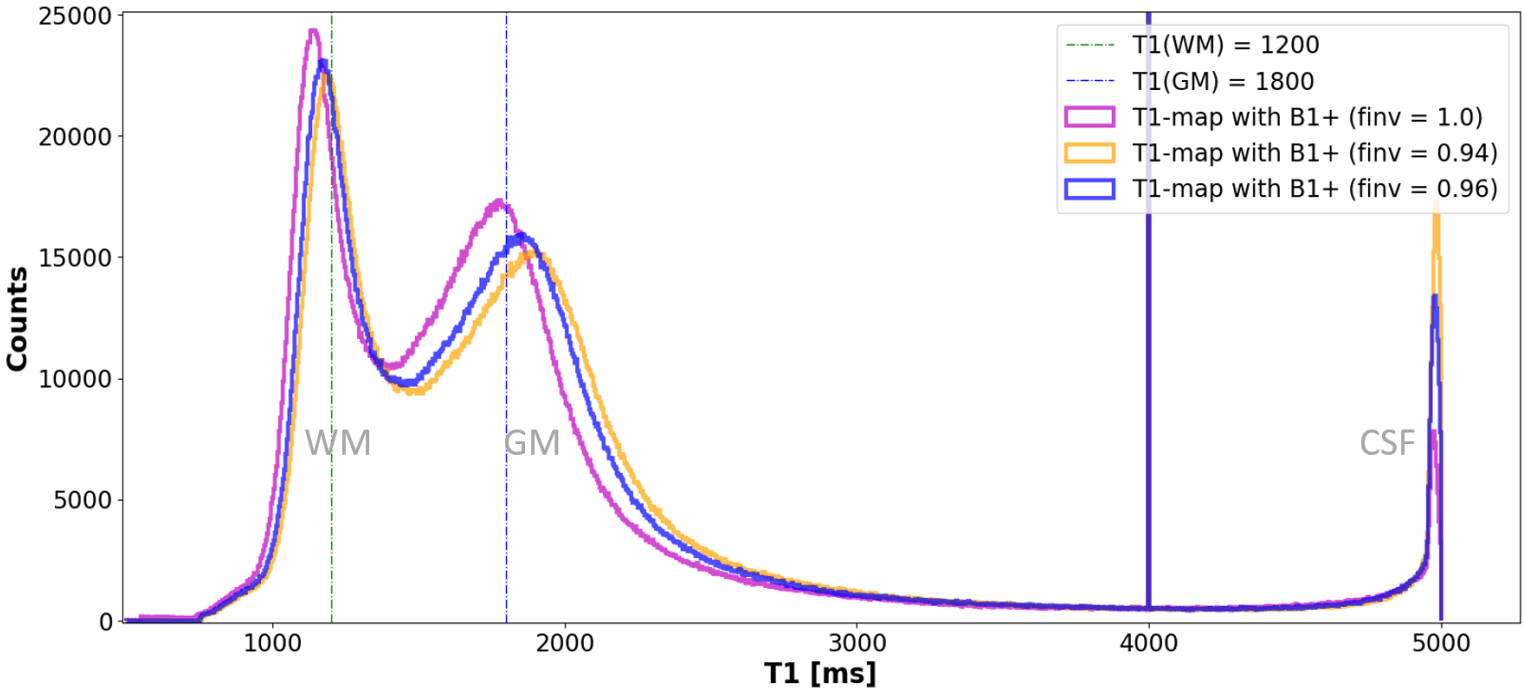

Fig. 19. A comparison of the corrected T1-maps for different assigned f_{inv}. The selected f_{inv} = 0.94 value offers a closer WM-peak to the theoretical T1 value for WM (1200 ms) and a broader GM peak, further away from the theoretical GM T1 value (1800 ms). Additionally, a higher CSF peak is observed in comparison to the other assigned f_{inv} -values.

Since the effect of the B_1^+ correction and a modified f_{inv} on the calculated T1-maps are known by now, it is of interest to proceed to investigate the influence of other variables on the corrected T1-map's accuracy. An example of such a variable is the amplitude of the adiabatic pulse, B_1-max.

4.4 The influence of the inversion pulse amplitude on the corrected T1-map accuracy.

4.4.1 Variation of B1-max

To assure inversion in low B_1^+ regions, the adiabatic inversion pulse requires the highest available B_1 ("Full adiabatic", B_1-max is typically 18μT).

The T1- (obtained at TI_1) and PD-weighted (obtained at TI_2) images acquired in experiment 1 for a range of different B_1-max values, based on the protocol in Table 1, are shown in Fig.(20). In this experiment, the B_1-max of the "Full adiabatic" inversion pulse is adjusted prior to each scan. Lower structural details are observed in the TI_1 images around the lower regions of the brain (temporal lobe) while the TI_2 images appear alike with a reduced B1-max. Similar effect was observed in cerebellum (despite it not shown in the figure).

Next, a selection of ROIs in WM is used to study the influence of B_1-max on both the MP2RAGE image intensity and the calculated T1-values for f_{inv} = 0.96 as shown in Fig. (21-22). For this experiment, the B1-max is adjusted manually while the pulse duration is modified automatically by the scanner to maintain the nominal FA of 1800°. The maximum achievable B1-max by the scanner during this experiment was 16 µT.

In Fig. (21), The B_1-max variation appear to have greater influence on the MP2RAGE values around regions with low B_1^+ than around regions with high B_1^+. Additionally, the f_{inv} value seems to be increasing with increased B_1-max, more specifically around B_1^+ = 0.40 (very low B_1^+ regions).

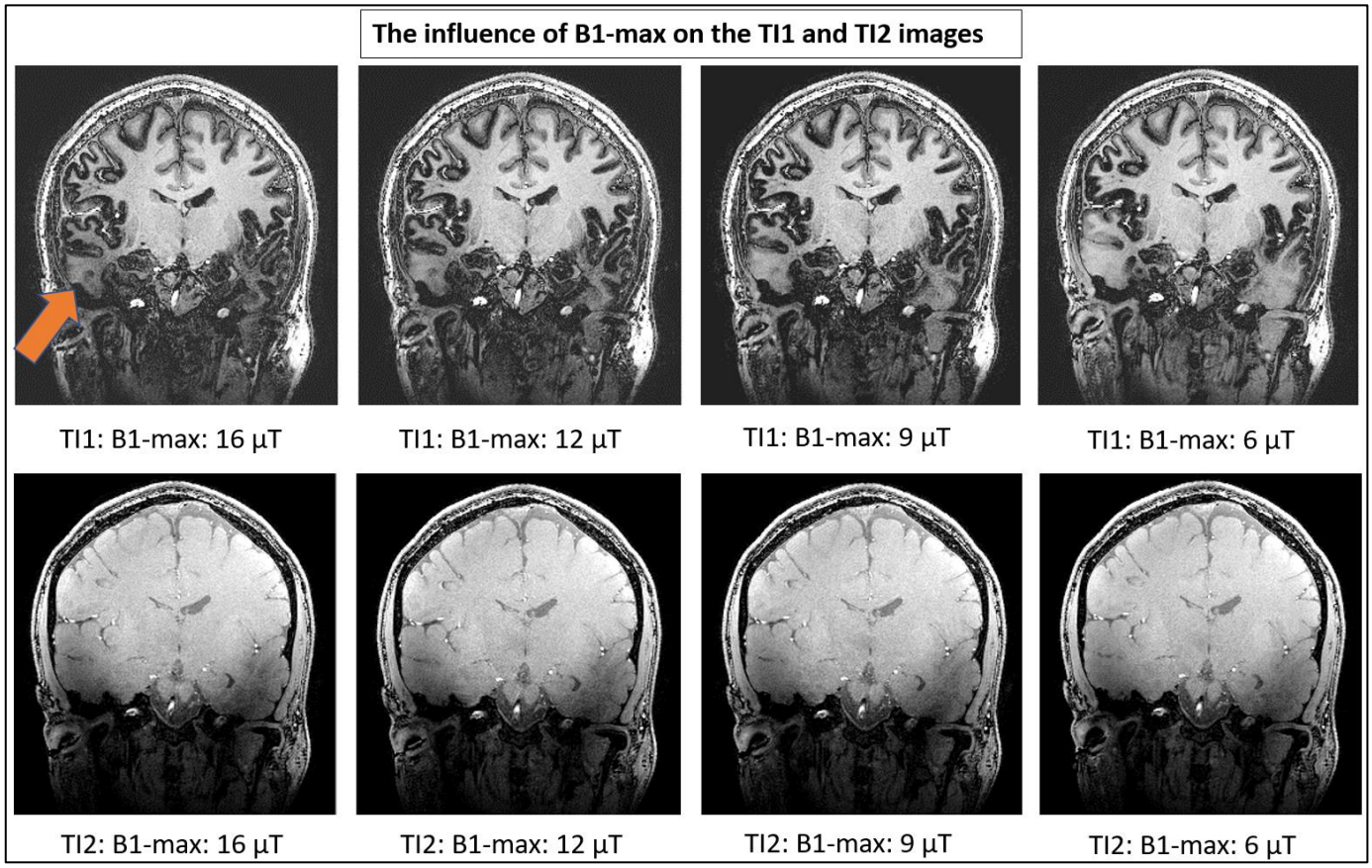

Fig. 20. Reduced adiabatic pulse amplitude (B_1-max) on the obtained images at TI_1 (S_1) and TI_2 (S_2). Lower structural details are observed in the TI_1 (T1-weighted) images around the lower regions of the brain (temporal loge) with a decreased B_1-max while the TI_2 (PD-weighted) images appear alike (not affected). The arrow points to the inferior temporal lobes. Similar effect was observed in cerebellum (not shown here).

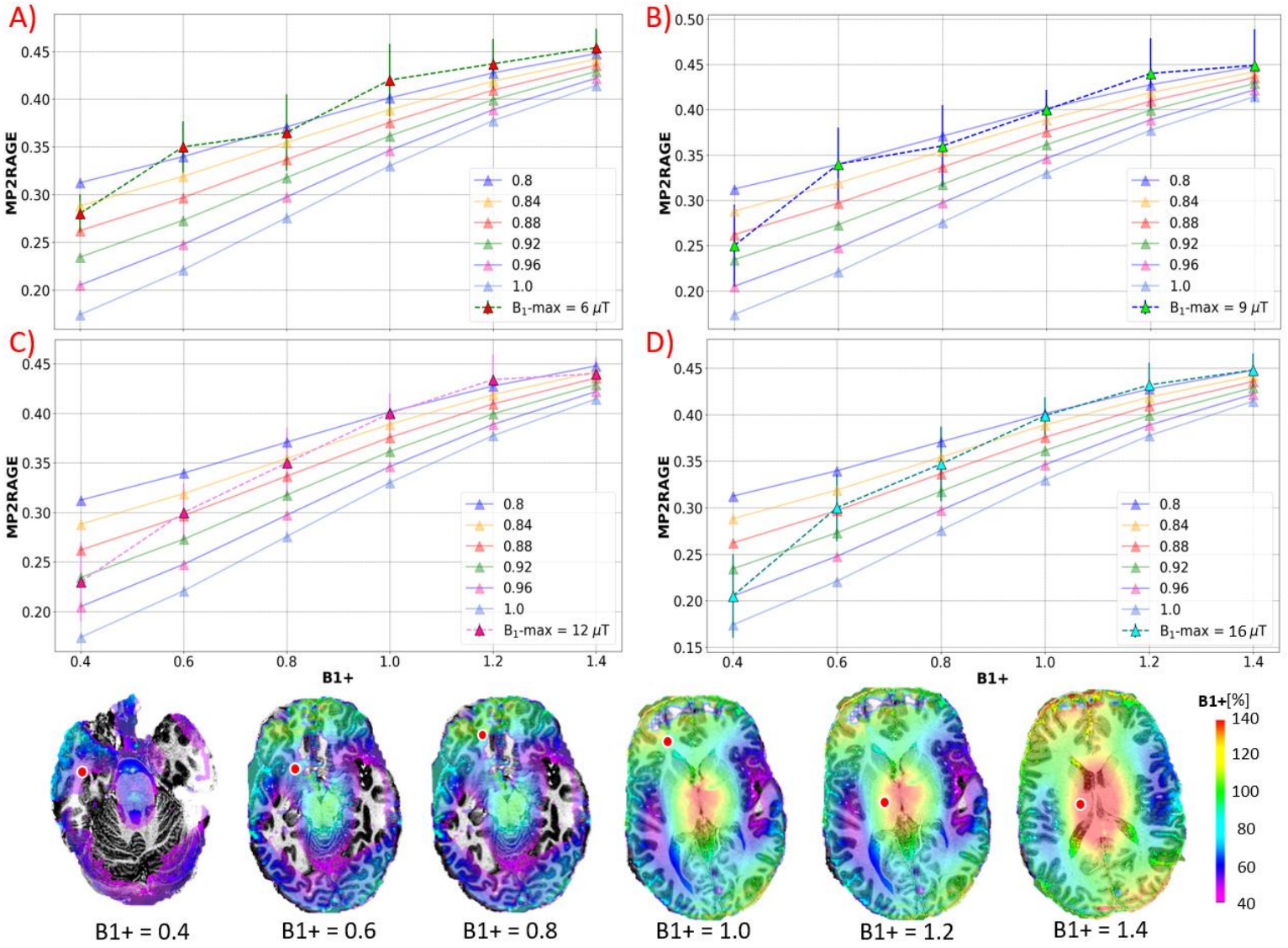

Fig. 21. The different B_1-max (A: 6 µT, B: 9 µT, C: 12 µT, and D: 16 µT) yields different datapoints on the MP2RAGE versus B_1^+ plots, obtained from ROIs (red) at several regions of WM across the brain. The B_1-max variation appear to have greater influence on the MP2RAGE values around regions with low B_1^+ than around regions with high B_1^+. The data points represent the mean in each ROI. The error bars indicate the standard deviation. The B_1^+ maps are obtained with B_1-max = 16 µT.

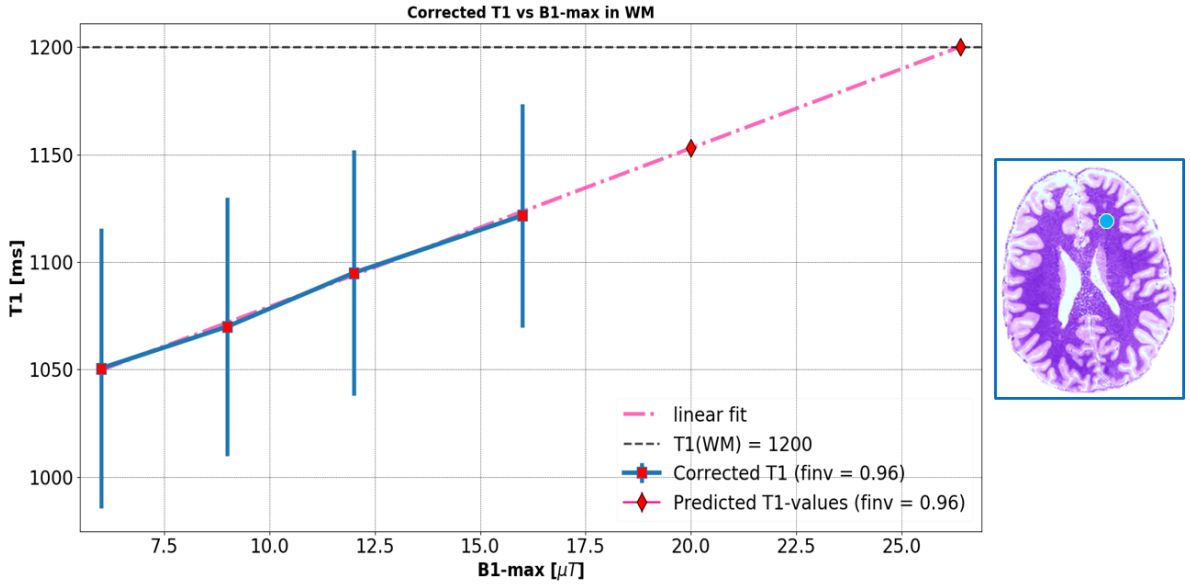

Fig. 22. The influence of increased B_1-max on the corrected T1-maps for f_{inv} = 0.96 measured in frontal WM (blue ROI). The extrapolation (pink) shows the expected T1-value that would have been obtained at a higher B_1-max of about 26 µT. The error bars indicate the standard deviation.

A linear fit is applied to obtain higher T1-values for higher B_1-max, due to constraints in reaching higher B_1-max by the scanner for test subjects with a relatively large head size. As observed, the predicted B_1-max value in order to reach the decided T1-value for WM is around 26 µT. The assigned f_{inv} is set to 0.96 (default value). Nonetheless, by utilizing f_{inv} = 0.94, higher T1 would have been acquired.

Moreover, the T1-value for B_1-max 6 µT was far off the expected T1-value of WM (1200 ms) given that the T1-maps are calculated with the assigned f_{inv} set to 0.96. Therefore, we investigate the possibility of reducing this deviation by assigning a set of different f_{inv} -values and conduct a ROI selection in WM and GM to study the effect on the T1-values as presented in Fig.(23).

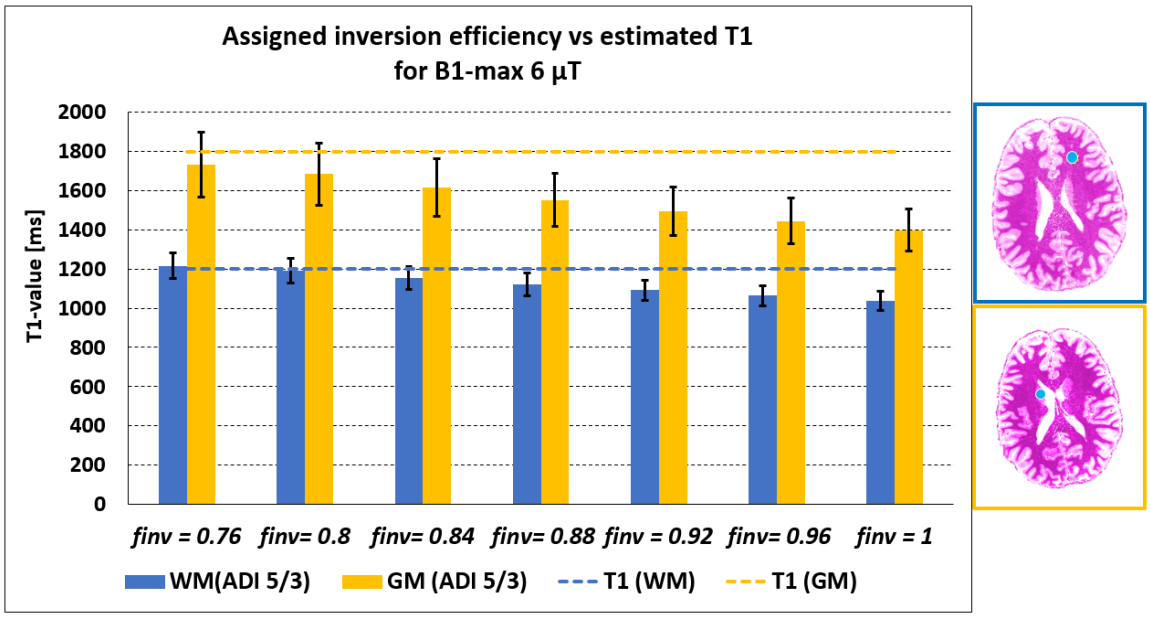

Fig. 23. An assigned f_{inv} = 0.8 brings the corrected T1-values in WM and GM for B_1-max = 6 µT the closest to their theoretical T1-values; 1200 ms and 1800 ms, respectively.

4.4.2 Experimental simulation of B_1^+ variation

From the results above, it is demonstrated that f_{inv} change with B_1-max which influence the accuracy of the T1-maps. The simulated change of B_1^+ allow us to maintain a constant location of the ROIs for different B_1-max images.

To simulate local changes of B_1^+, the B_1-max value was altered while maintaining the pulse duration constant at 17.1 ms (referring to nominal B_1-max of 18 µT and FA of 1800°).

The T1- and PD-weighted images (TI_1 and TI_2) are presented in Fig.(25). The decrease of B_1-max leads to T1-weighted images with decreased structural details/T1-contrast. Moreover, the PD-weighted images are only slightly affected by B_1-max. A global breakdown of inversion is observed at B_1-max= 3 µT.

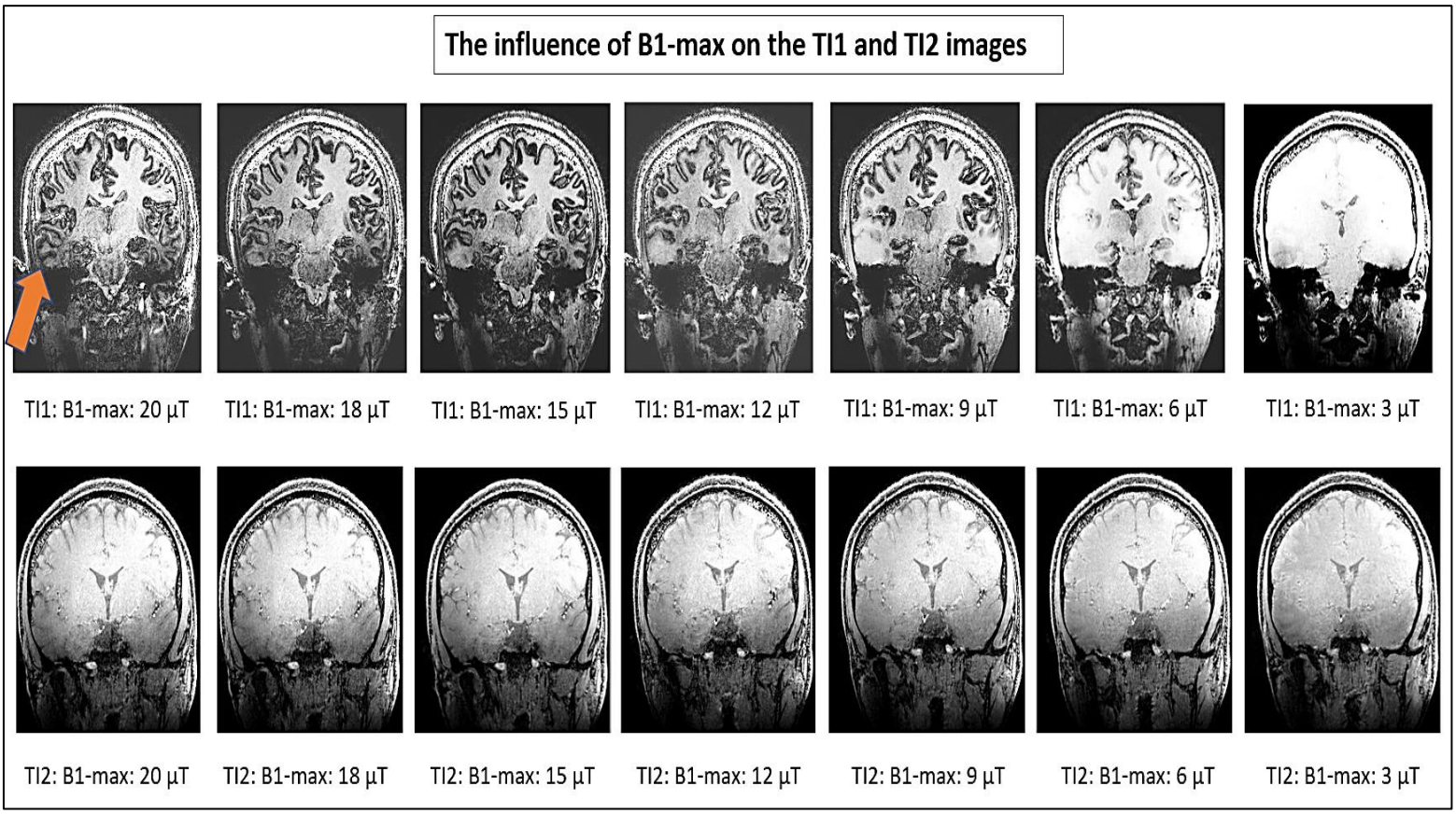

Fig. 24. Multiple T1-and PD-weighted images based on the MP2RAGE protocol provided in Table 1 of a test subject with average head size to obtain a broader range of B_1-max from 20 µT down to 3 µT. Improved structural detail is observed at increased B_1-max. A global breakdown of inversion is observed at B_1-max 3 µT. The arrow points to the inferior temporal lobe. The temporal lobe (left side) remains slightly effected even at B_1-max = 18 µT. The TI_2 -images appear influenced by the reduction of B_1-max. More specifically at extremely low B_1-max.

To analyze the influence of a varying B_1-max on the corrected T1-maps, a group of ROIs (red) are selected in WM at the same region of the brain to obtain a T1 versus B_1-max plot presented in Fig.(25).

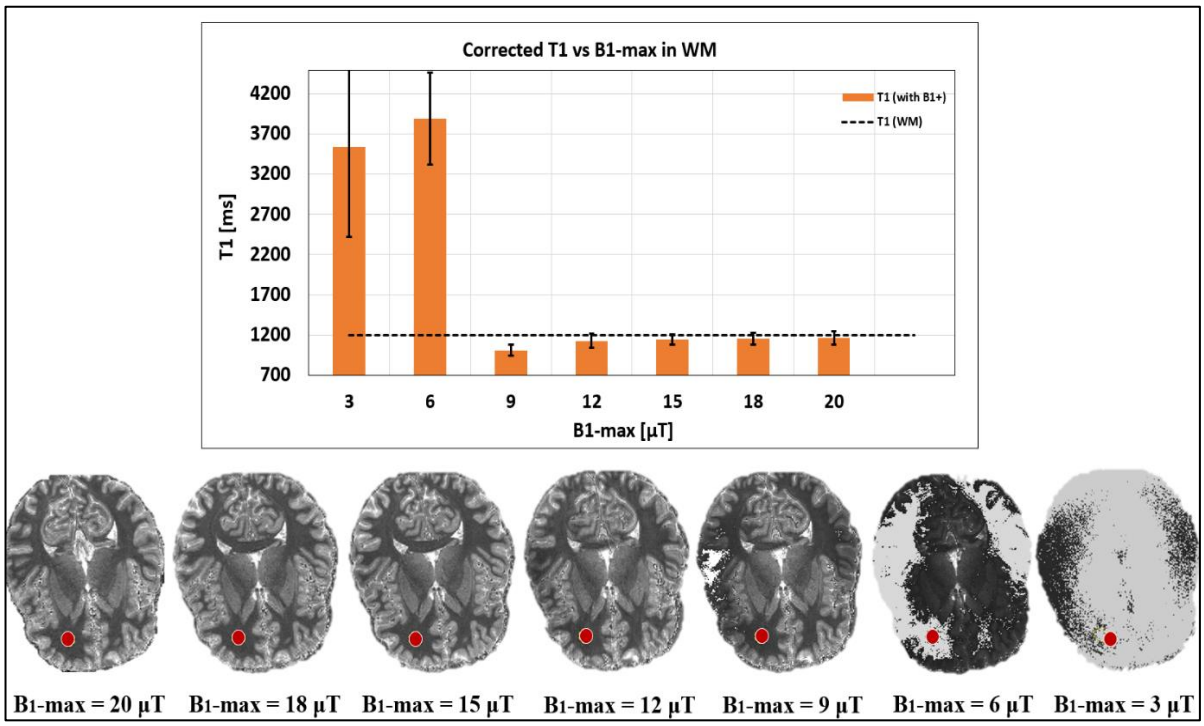

Fig. 25. Placement of ROI (red) for different B_1-max values to study the influence of a varying B_1-max on the accuracy of the corrected T1-maps for the default f_{inv} = 0.96. Note that the brain images are rotated in this figure.

As shown in Fig. (25), the very low B_1-max values (3 µT and 6 µT) leads to a large deviation from the reference T1-value for WM in comparison to the remaining ROI values. Therefore, a second plot focusing on the B_1-max values from 9µT up to 20 µT is presented in Fig. (26). Additionally, the same principle for readjusting f_{inv} for the lowest B_1-max (9 µT) is followed. To find a proper f_{inv} carrying the T1-values closer to the selected T1-value for WM. The found f_{inv} is 0.7.

Moving on, we seek to create a f_{inv} versus B_1^+ plot to investigate if any relationship exists in between. To do so, the ROIs presented in Fig.(25) for each B_1-max are acquired for a range of f_{inv} values [0.7 – 1.0] to estimate a suitable f_{inv} (bringing the T1-values closest to the reference T1-value of WM/GM) for each B_1-max. Next, these f_{inv} are plotted versus the relative B_1^+ (B_1^{+*}) of corresponding ROI as illustrated in Fig.(27). The B_1^{+*} is calculated according to

$$B_1^{+*} = B_1^+ \cdot \frac{B_1 max}{B_{1_{ref}}}, \qquad (16)$$

Where, $B_{1_{ref}}$ = 18 µT corresponds to the reference value of B_1-max and thus the nominal B_1^+-value at the ROI. The results are presented in Fig.(27).

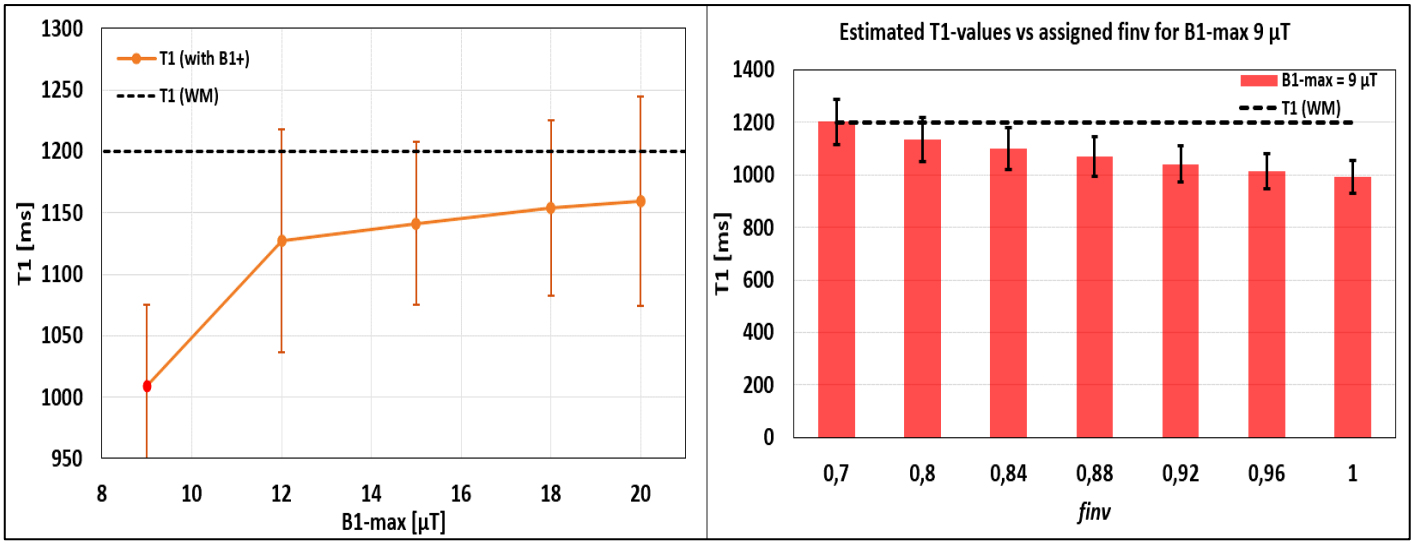

Fig. 26. To the left, a closer view of the estimated T1 versus B_1-max over an interval of 9µT to 20 µT for the WM ROI in Fig. (25). On the right-hand side, the assigned $f_{inv} = 0.7$ brings the corrected T1-values in WM for B_1-max = 9 µT the closest to the expected T1-value of WM.

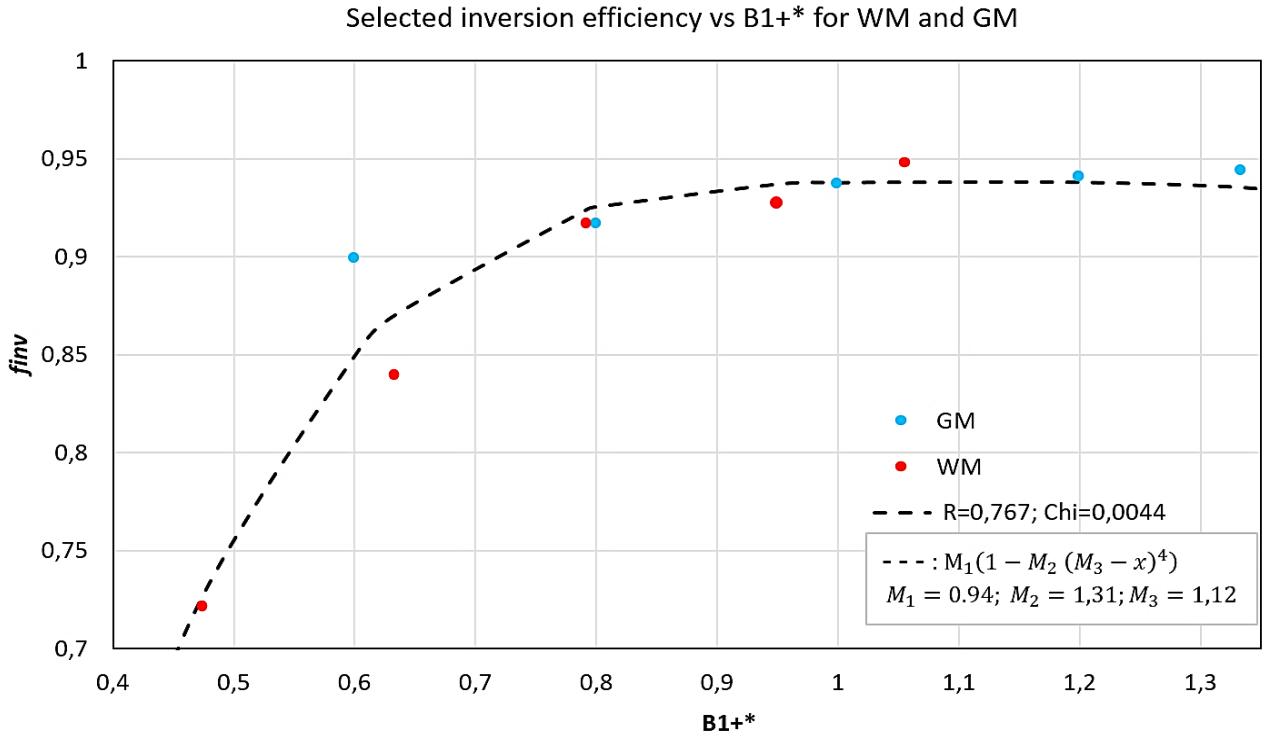

Fig. 27. The suitable f_{inv} versus the relative B_1^{+*} obtained from selecting the f_{inv}-value corresponding to the closest T1-value to the reference T1 of WM and GM (1200 and 1800 ms). The T1 for GM is measured in the caudate nucleus. A plateau around $f_{inv} = 0.94$ is starting to form for $B_1^{+*} > 0.9$.

The non-linear fit equation presented in Fig.(27) is the following:

$$Y(x) = M_1(1 - M_2(M_3 - x)^4). \qquad (17)$$

Here, M_1, M_2 and M_3 are constant determined to 0.94, 1.31 and 1.12, respectively.

4.5 Comparison of two adiabatic pulses and protocols on inversion efficiency and B_1^+ sensitivity

The maximum possible B_1-max is 12 μT for this experiment due to the test subject's larger head size.

4.5.1 Comparison of adiabatic pulse types

The obtained results using the full adiabatic and FOCI pulses for α_1^o/α_2^o = 5º/ 3º are presented in Fig. (28). As observed in the figure, an improved structure definition of the cerebellum is obtained with the FOCI pulse in comparison to the full adiabatic pulse for the same protocol parameters.

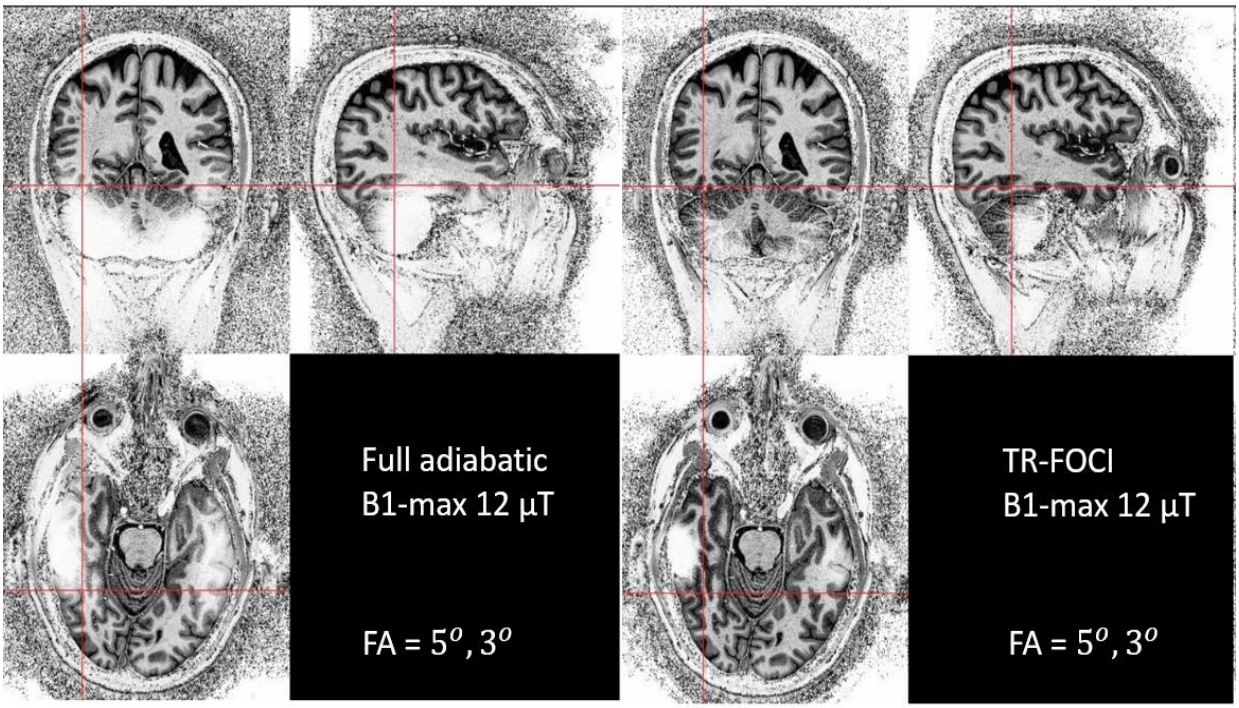

Fig. 28. Comparison of the full adiabatic and the FOCI pulses for the protocol provided in Table 1 for B_1-max=12 μT (enforced by coil loading). Note that only the flip angle of 2250º, but not B_1-max can be chosen for the FOCI pulse. An improved structure definition is obtained in the lower region of the brain using the FOCI pulse.

4.5.2 Protocol comparison

A protocol comparison based on Table 2 is performed in between the α_1^o/α_2^o = 5º/3º and α_1^o/α_2^o = 4º/5º using the same sequence timings and FOCI pulses of 2250º as presented in Fig. (29). The protocol with α_1^o/α_2^o = 4º /5º provides less contrast between WM and GM although better structure definition is maintained in the lower regions of the brain. That is, the artifacts are reduced in low B_1^+ regions.

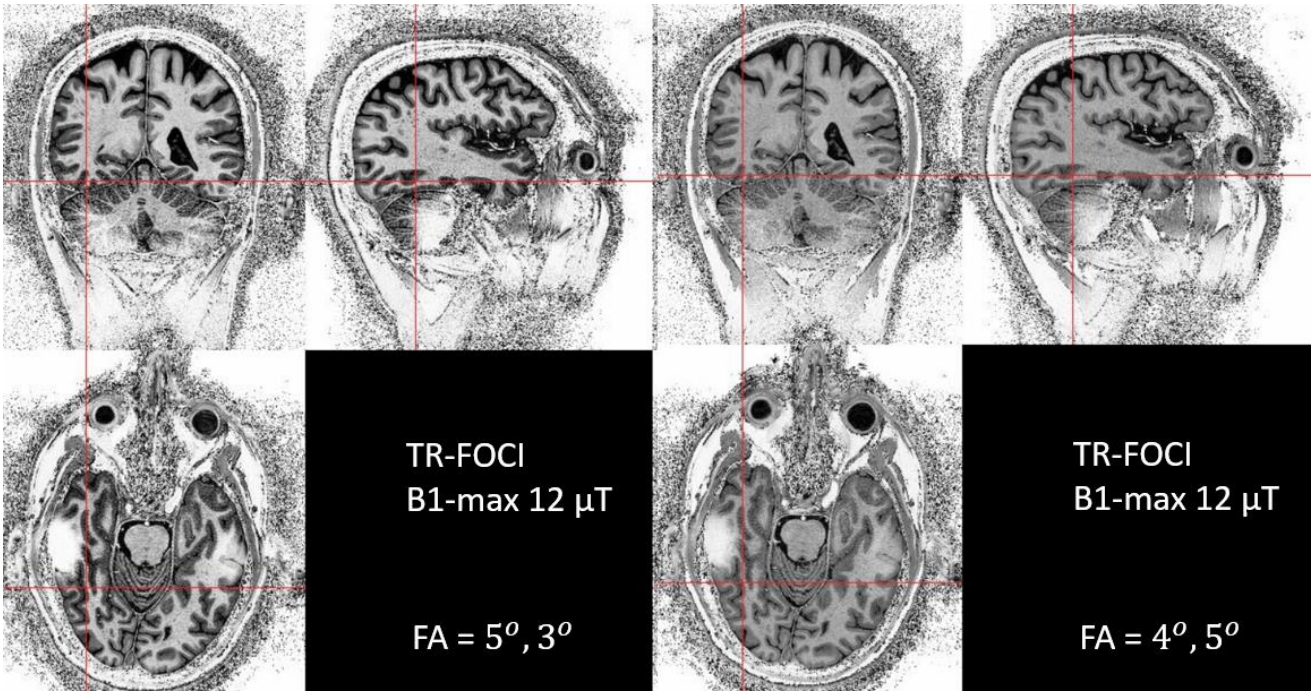

Fig. 29. Comparison of the FOCI pulses impact on the MP2RAGE images applied with different flip angles. In which the α_1^o/α_2^o = 4^o / 5^o protocol provided less contrast between the WM and GM. Additionally, both protocols maintained structure definition in the cerebellum.

The simulation of the protocols above returned an MP2RAGE versus T1 plot, shown in Fig. (30). A larger B_1^+ sensitivity is observed in the 5^o/3^o –protocol (1a) in comparison to the 4^o/5^o–protocol (1b) for similar range of different B_1^+-values and a default f_{inv} = 0.96.

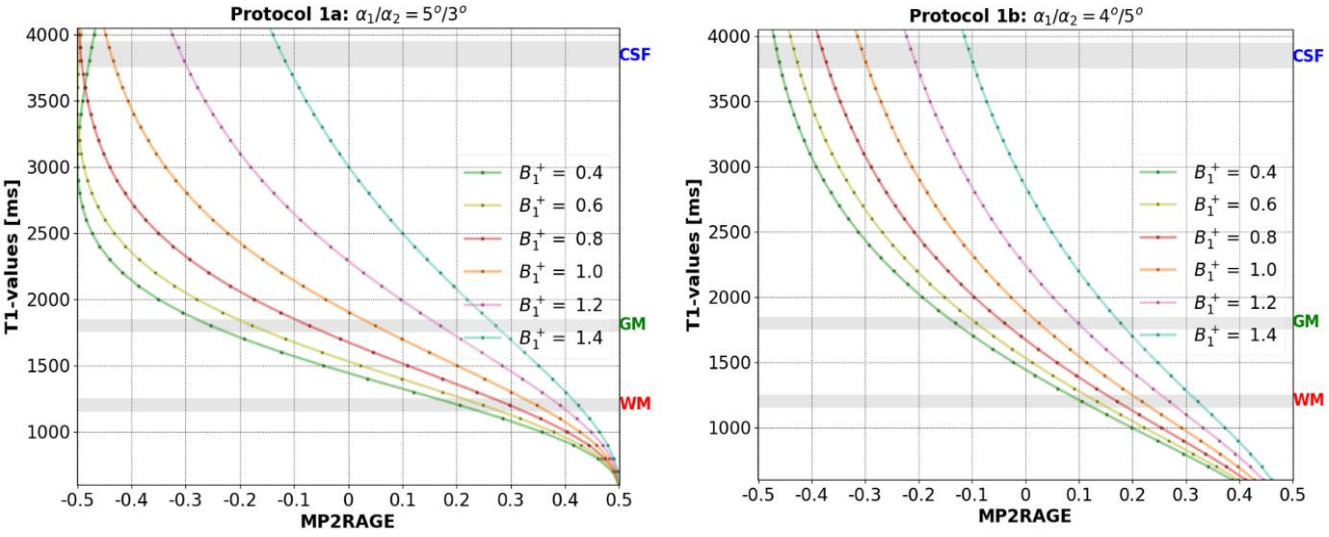

Fig. 30. The B_1^+ sensitivity of different protocols on the mapping of MP2RAGE to T1-values. Protocol 1a) is based on Table 1 and protocol 1b) is the same except for the flip angles. A diminished B_1^+ sensitivity in particular GM is observed.

4.5.3 T1-mapping and the selection of inversion pulse type

The influence of the different protocols and pulse types in Table 2 on the corrected T1-maps in WM and GM for B_1-max = 12 µT and different assigned f_{inv} is presented in Fig.(31). The selected ROI values in WM and GM are obtained by overlaying two slices with different f_{inv} on each other.

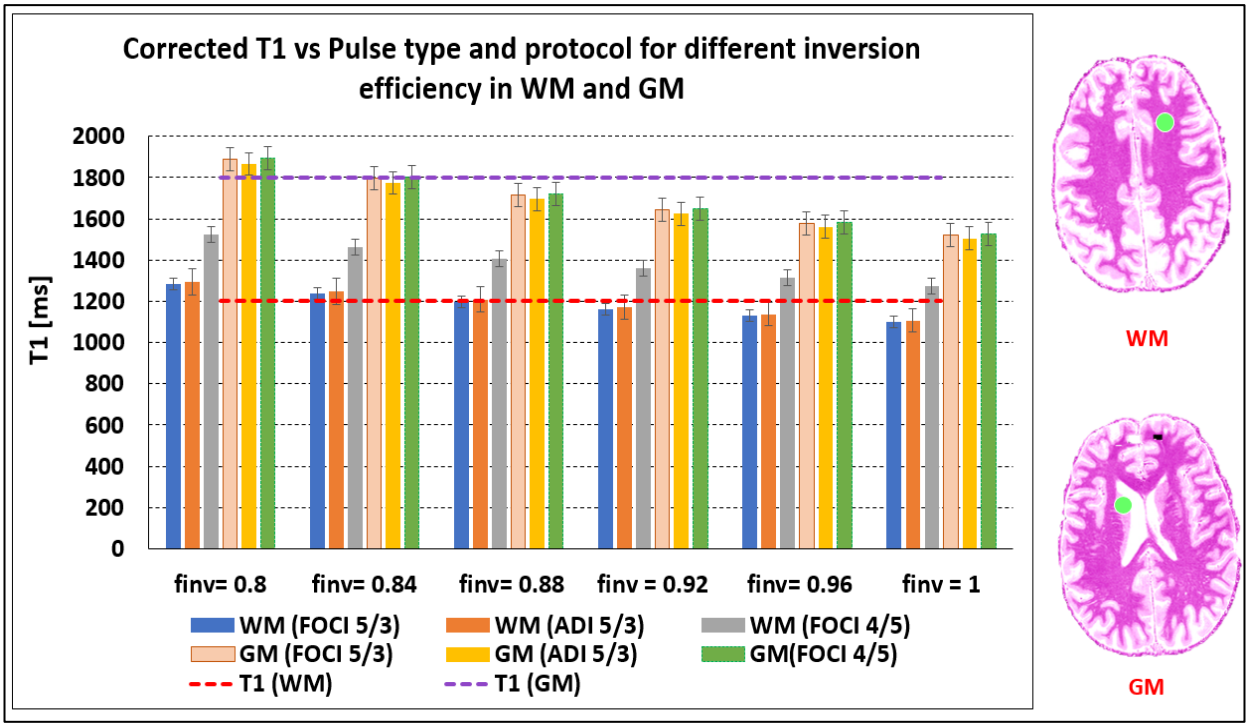

Fig. 31. Corrected T1-values obtained from the selected ROIs (green) for different f_{inv} values, pulse types and protocols (Table 2) in WM and GM for B_1-max = 12 µT (enforced by coil loading). The B_1^+ in the ROIs was approximately 120% in GM and 100% in WM.

Shown above, the FOCI protocol with α_1^o/α_2^o = 4°/5° (FOCI 4/5, gray) produces high T1 values in WM for all the different assigned f_{inv} relative to the 5°/3° -protocol (FOCI 5/3, blue). However, the GM T1 (green) appears similar to the T1 values obtained with the FOCI 5/3- protocol (light pink). Moreover, the suitable f_{inv} for the FOCI 5/3-protocol appears to be around 0.84. While for the FOCI 4/5-protocol it is around 1.0 for an improved WM T1-accuracy and around 0.84 for an improved GM T1-accuracy. As for the ADI 5/3-protocol, the suitable f_{inv} seems to be around 0.84 for WM and GM.

5 Discussion

5.1 The B_1^+ correction and assigned inversion efficiency

As observed in Fig. (10), calculation of T1-maps with a separately acquired B_1^+-map for correction mitigates potential systematic errors across the brain. Hence, more reliable T1-maps at UHF can be obtained by utilizing a B_1^+-map correction. The more prominent transmit B_1^+ field inhomogeneity at UHF is a consequence of the shortened radiofrequency wavelength in the tissue, meaning that it is smaller or on the same order of magnitude as the size of the head [35]. Note that the MP2RAGE protocol used here was optimized for speed [28], not for cancellation of B1+ effects. Moreover, the original Philips software does not allow $\alpha_2 > \alpha_1$. This was only achieved by an in-house software modification (Hampus Olsson).

By studying the histograms (Fig.(11 and 13)) of both the corrected and uncorrected T1-images, it is obvious that the CSF peak value seems lower than proposed in literature [2]. So far, we have no explanation to this. The CSF T1-value appear not to be very susceptible to variation of the inversion efficiency factor assigned for T1-mapping as observed in Fig. (13 and 19). Due to its long T1, the inversion in CSF is near ideal (no relaxation during the pulse duration). By selecting a lower f_{inv} than 1.0, like for instance 0.94, the simulated CSF relaxation begins at a higher M_z, so the experimental S_{TI_1} will be misleading. Furthermore, the flow of CSF in the brain might also influence its T1 value. As it is not constant across the brain but rather spatially dependent (how much tissue surrounding the flow). Around the edges of the brain (few surrounding tissues) CSF seems to show lower T1-values than around the middle of the brain (more surrounding tissues). Lastly, partial volume effects are also present and may influence the T1 value, more specifically near the edges of the tissues.

Around the cerebellum/temporal lobes, there exist some very bright pixels that conceal the anatomy of the regions at low B_1^+-values (around 20-30 % of the nominal FA) due to failed inversion at the region. These areas require higher B_1-max (may be limited by the RF hardware). Nonetheless, an improvement can be achieved by utilizing the FOCI pulse.

When the T1-maps are calculated, a global f_{inv} is assumed/assigned in the code. Therefore, a method enabling adjustment of f_{inv} on a pixel-level based on B_1^+ is needed to achieve higher accuracy of T1, especially around the lower regions of the brain. To do so, a simulation tool (like our tool) taking account of B_1^+ and f_{inv} influence on the pixel-level is of importance. Fig. (27) shows such an attempt in single ROI.

The images presented in Figs. (20 and 24) show certain spots that appear very bright. These spots belong to arteries, allowing the inflow of unsaturated M_z close to M_0 to be picked up by the RAGE readout. As the spin of new blood is less/not affected by the inversion of M_z, it displays higher signal in the image and therefore appear bright.

5.2 Simulations

All the simulations for M_z and the consecutive MP2RAGE signal are coded in Python and constructed based on the assumption that the T1-values for WM, GM, and CSF are 1200 ms, 1800 ms and 4000 ms, respectively. From literature [2] we are aware that our selected GM T1 value is a bit high. Nonetheless, by selecting such a high value we are certain that the simulation corresponds to the heterogeneous GM tissue. Moreover, a limited range of B_1^+-values between 40 % -140 % is used. However, there might exist higher and lower B_1^+-values that were not taken into consideration in our simulation. The effect of inhomogeneous B_1^+ is clearly observed on the M_z and MP2RAGE signal in Fig.(15), where the very low B_1^+ corresponds to low M_z around TI_1 and high M_z around TI_2 for the given protocol in Table 1. This behavior is observed in all the three tissues. However, for CSF, the T1-value is far greater than that for WM and GM leading to a different MP2RAGE vs B_1^+ plot (Fig.(17)), where no increase of MP2RAGE is observed with increased B_1^+, up to $B_1^+ \approx 0.8$.

Regarding the inversion efficiency behavior presented in Fig. (17-18), the largest deviation of MP2RAGE signal for different f_{inv} is observed at low B_1^+. This is because the MP2RAGE signal already suffer from the reduced value of B_1-max. On the other hand, the difference in MP2RAGE signal due to f_{inv} seems to get smaller around pixels/regions with high B_1^+. It appears that variation of f_{inv} does not yield a large variation of the MP2RAGE signal at high B_1^+ regions.

The MATLAB script provided by J.P. Marques [33] calculates the MP2RAGE signals for a range of T1-values being [500 ms-5000 ms]. However, in our MP2RAGE versus T1 simulations the maximum value was set to be 4000 ms based on the assumption that any higher T1-value will be assigned to CSF. Otherwise, the simulations appear comparable, and indicate that utilizing only the M_z relaxation equations yield satisfactory results that are comparable to the simulations based on the advanced Bloch equations, as shown in Fig.(32) in appendix section 8.1.

The conducted simulations provide an insight into the M_z dynamics behind MP2RAGE, facilitating investigation into the influence of B_1^+ and f_{inv} on the MP2RAGE/T1-maps, and opens the door for further research based on visualizing different MP2RAGE protocols. The code is also able to simulate up to MPXRAGE (MP3RAGE, MP4RAGE, etc.) by concatenating the above Eqs. (7-11). The used Python code to simulate the MP2RAGE protocols can be found on GitHub [29].

5.3 Estimation of the inversion efficiency factor

As a first approach to estimate the inversion efficiency factor (f_{inv}), a scatter plot of the MP2RAGE pixel values versus their corresponding B_1^+-values was investigated for a distinct correlation. However, no significant correlation could be attained from the plot and the method is regarded as an unsuccessful approach to estimate $f_{inv.}$ A major cause for this is the amount of noise in the MP2RAGE images and present partial volume effects that influence the distribution of the pixel values in respect to the B_1^+-values. We then directed our approach to estimate f_{inv} by utilizing several ROIs across the brain at different B_1^+ to obtain simultaneous readout of the pixel intensity and corresponding B_1^+-value. Despite the initial success of this method in finding suitable f_{inv} as demonstrated in Fig.(18), it is time consuming, sensitive to placement and size of the ROI.

To avoid moving the ROIs across the brain when measuring MP2RAGE/T1-values for different B_1^+, we experimentally simulated the effect of varying B_1^+ by varying B_1-max in each MP2RAGE acquisition. The presented result concerning f_{inv} in Fig. (27) is of importance as it illustrates that for pixel values affected by low B_1^+, the value of f_{inv} needs to be adjusted to obtain accurate T1. While for regions with $B_1^+ > 100\%$, the suitable f_{inv}-value appears approximately constant for increasing B_1^+. Now that a function of the real f_{inv} is known for respective values of B_1^+ (Fig. (27)), a correction on a pixel-wise level can be conducted in future work. Moreover, the suitable f_{inv} seems to be similar for both WM and GM. Implementation of a $\boldsymbol{f_{inv}(B_1^+)}$ function is desirable to improve the global T1-accuracy for both tissue types. This is an advanced B_1^+ correction for f_{inv}, but cannot account for failure of inversion in regions where the local B_1-max falls below what is required to fulfill the adiabatic threshold. Due to limited time to conduct this thesis work, the f_{inv} in CSF was not estimated (it is also not as interesting as WM and GM). However, we know that it is not very susceptible to variation of f_{inv} and might not require such advanced correction.

One of the big challenges with estimating a reliable f_{inv} concerns the dependence of the estimation on the assumed T1-value. And in reverse, accurately estimated T1-values rely on a reliable adjustment of assigned f_{inv}. Thus, the empirical adjustment of f_{inv} is not a trivial task. So far, there is variation in the published T1 values for WM, GM, and CSF in UHF scanners. Furthermore, a potential weakness is that we did not use a reference T1 mapping method, such as a conventional IR experiment.

Unsuitable assignment of f_{inv} may display longer/shorter T1 than expected. Additionally, the impact of persisted bias of B_1^+ on the accuracy of the T1-maps remains larger than the impact of selecting the default f_{inv} (0.96; proposed by literature [3][34]) despite it not being the optimal one. This impact depends on the sequence protocol. In this study, we observed f_{inv} as low as $f_{inv} = 0.8$ due to the worse performance of the "Full adiabatic" pulse relative the FOCI pulse and rather low B_1-max achievable by the Philips RF system. The extrapolation in Fig. (22) shows that a B_1-max = 26 µT is required. Which is about twice the B_1-max achievable in this subject.

5.4 Influence of the adiabatic inversion pulse amplitude on the corrected T1-map accuracy

In addition to the dependence of f_{inv} on the accuracy of the reference T1-values for respective tissues, estimated T1 also depends on the inversion pulse characteristics: such as its type (more on this in the next subsection), duration, and maximum amplitude (B1-max). During the inversion of M_z, T2-relaxation is present and might reduce the efficiency of the inversion due to dephasing, in case the pulse duration is equivalent/close to the T2-value [36]. For the UHF scanners, the T2-value tends to be shorter than at 3T/1.5T scanners in both intra/extracellular and myelin water (MW) [37]. Specifically, at 7T, the T2-values for WM and GM are approximately 50 ms (MW: 3-20 ms) and 39-48 ms [37][38]. The length of the adiabatic pulse used to obtain Fig. (24) was equivalent to 17.1 ms.

The value of B_1-max is of importance mainly to satisfy the adiabatic condition (Eq. (15)). By satisfying the condition the total inversion efficiency improves across the brain as presented in Fig. (24).

Unfortunately, the adiabatic condition is not always met in UHF scanners due to low B_1^+. Same problem occurs when dielectric pads are used (or when running the dual transmit channel setup in quadrature mode). If the maximum peak power is exceeded, the value of B_1-max is reduced, which may influence the inversion factor, f_{inv}.

Moreover, the rather short length of the head transmit coil compared to the model used on the Siemens scanners [28] can lead to poor coverage of the lower regions of the cerebellum and reduced inversion efficiency. This returns increased T1-values. A potential solution for this can be either further increasing B_1-max or the utilization of different pulse types.

5.5 Comparison of two adiabatic pulse shapes and protocols on inversion efficiency and B_1^+ sensitivity

A major distinction between the "Full adiabatic" and the FOCI pulses, is the capability of the FOCI pulse to improve the inversion efficiency/coverage of the low B_1^+ regions of the brain (e.g. Cerebellum and temporal lobes), as shown in Fig.(28). What enables the FOCI pulse to achieve better inversion at lower B_1^+ is yet not fully understood by us. Nonetheless, for an improved lower brain coverage, the FOCI-pulse is recommended to be employed.

An example of different imaging protocols and their influence on image quality and derived T1-maps is shown in Figs. (29-31). The MP2RAGE images obtained with the FOCI pulse and the $4^o/5^o$-protocol have lower WM-GM contrast in comparison to the $5^o/3^o$-protocol. A potential cause of this is that TI_1 and TI_2 have been optimized for $5^o/3^o$ and needs to be readjusted for $4^o/5^o$. The latter protocol mitigated the manifestation of B_1^+-inhomogeneities as predicted by the simulation in Fig. (30). Additionally, it is still to be determined if the $4^o/5^o$ yields more homogeneous images before the B_1^+ correction. Moreover, the obtained contrast appears to be independent of B_1^-, T2*and M_0 as promised by the MP2RAGE concept.

As noted, the optimization of mutually independent protocol parameters plays a major role here. Adjustments of the FAs alone might lead to creating MP2RAGE/T1-maps images that are less susceptible to the B_1^+ inhomogeneity. Thus, it is important to consider optimizing the FA of the MP2RAGE protocols at UHF where the B_1^+ variations tend to be more prominent.

In the MP2RAGE protocols there are additional parameters beside the FA that would be of interest to investigate such as: TI_1/TI_2, TR and $MP2RAGE_{TR}$. The feature of low/high FA was implemented only during the course of the thesis work. The results prepare for further optimization of the MP2RAGE protocol and T1-mapping at UHF.

6 Summary

The use of separately acquired B_1^+ map improved the reliability of the protocol-specific T1-maps. By applying the FOCI pulse, the inversion efficiency could be improved around the inferior low B_1^+ regions of the brain. When using the standard "Full adiabatic" inversion instead of the FOCI pulse, the maximum amplitude of the adiabatic pulse should be as high as allowed by the scanner to ensure maximum inversion efficiency. Lastly, assigned f_{inv} needs to be adjusted to B_1-max when estimating T1, ideally as a function of B_1^+.

7 References

[1] M. F. Callaghan, G. Helms, A. Lutti, S. Mohammadi, and N. Weiskopf, "A general linear relaxometry model of R1 using imaging data," *Magn. Reson. Med.*, vol. 73, no. 3, pp. 1309–1314, 2015, doi: 10.1002/mrm.25210.

[2] W. D. Rooney *et al.*, "Magnetic field and tissue dependencies of human brain longitudinal 1H2O relaxation in vivo," *Magn. Reson. Med.*, pp. 308–318, 2007, doi: 10.1002/mrm.21122.

[3] J. P. Marques, T. Kober, G. Krueger, W. van der Zwaag, P. F. Van de Moortele, and R. Gruetter, "MP2RAGE, a self bias-field corrected sequence for improved segmentation and T1-mapping at high field," *Neuroimage*, pp. 1271–1281, 2010, doi: 10.1016/j.neuroimage.2009.10.002.

[4] P. F. Van de Moortele, E. J. Auerbach, C. Olman, E. Yacoub, K. Uğurbil, and S. Moeller, "T1 weighted brain images at 7 Tesla unbiased for Proton Density, T2* contrast and RF coil receive B1 sensitivity with simultaneous vessel visualization," *Neuroimage*, pp. 432–446, 2009, doi: 10.1016/j.neuroimage.2009.02.009.

[5] H. Olsson, M. Andersen, J. Lätt, R. Wirestam, and G. Helms, "Reducing bias in dual flip angle T1-mapping in human brain at 7T," *Magn. Reson. Med.*, pp. 1347–1358, 2020, doi: 10.1002/mrm.28206.

[6] N. Bloembergen, E. M. Purcell, and R. V. Pound, "Relaxation effects in nuclear magnetic resonance absorption," *Phys. Rev.*, pp. 679–712, 1948, doi: 10.1103/PhysRev.73.679.

[7] H. C. Moon, H.-M. Baek, and Y. S. Park, "Comparison of 3 and 7 Tesla Magnetic Resonance Imaging of Obstructive Hydrocephalus Caused by Tectal Glioma," *Brain Tumor Res. Treat.*, pp. 150–154, 2016, doi: 10.14791/btrt.2016.4.2.150.

[8] A. G. Van Der Kolk, J. Hendrikse, J. J. M. Zwanenburg, F. Visser, and P. R. Luijten, "Clinical applications of 7 T MRI in the brain," *European Journal of Radiology*. pp. 708–718, 2013, doi: 10.1016/j.ejrad.2011.07.007.

[9] S. L. Paek *et al.*, "Early experience of pre- and post-contrast 7.0T MRI in brain tumors," *J. Korean Med. Sci.*, pp. 1362–1372, 2013, doi: 10.3346/jkms.2013.28.9.1362.

[10] C. M. Collins and M. B. Smith, "Signal-to-noise ratio and absorbed power as functions of main magnetic field strength, and definition of '90°' RF pulse for the head in the birdcage coil," *Magn. Reson. Med.*, vol. 45, no. 4, 2001, doi: 10.1002/mrm.1091.

[11] B. Hansson *et al.*, "Subjectively Reported Effects Experienced in an Actively Shielded 7T MRI: A Large-Scale Study," *J. Magn. Reson. Imaging*, pp. 1265–1276, 2020, doi: 10.1002/jmri.27139.

[12] M. E. Ladd *et al.*, "Pros and cons of ultra-high-field MRI/MRS for human application," *Progress in Nuclear Magnetic Resonance Spectroscopy*. pp. 1–50, 2018, doi: 10.1016/j.pnmrs.2018.06.001.

[13] H. Alizai, G. Chang, and R. R. Regatte, "MR Imaging of the Musculoskeletal System Using Ultrahigh Field (7T) MR Imaging," *PET Clinics*. pp. 551–565, 2018, doi: 10.1016/j.cpet.2018.05.008.

[14] G. Chang, L. Wang, A. Cárdenas-Blanco, M. E. Schweitzer, M. P. Recht, and R. R. Regatte, "Biochemical and physiological MR imaging of skeletal muscle at 7 Tesla and above," *Semin. Musculoskelet. Radiol.*, pp. 269–278, 2010, doi: 10.1055/s-0030-1253167.

[15] R. Deichmann, C. D. Good, O. Josephs, J. Ashburner, and R. Turner, "Optimization of 3-D MP-RAGE sequences for structural brain imaging," *Neuroimage*, pp. 112–127, 2000, doi: 10.1006/nimg.2000.0601.

[16] J. P. Mugler and J. R. Brookeman, "Three-dimensional magnetization-prepared rapid gradient-echo imaging (3D MP RAGE)," *Magn. Reson. Med.*, pp. 152–157, 1990, doi: 10.1002/mrm.1910150117.

[17] K. L. Miller, R. H. N. Tijssen, N. Stikov, and T. W. Okell, "Steady-state MRI: Methods for neuroimaging," *Imaging in Medicine*. pp. 93–105, 2011, doi: 10.2217/iim.10.66.

[18] A. Haase, J. Frahm, D. Matthaei, W. Hanicke, and K. D. Merboldt, "FLASH imaging. Rapid NMR imaging using low flip-angle pulses," *J. Magn. Reson.*, pp. 258–266, 1986, doi: 10.1016/0022-2364(86)90433-6.

[19] K. R. O'Brien *et al.*, "Robust T1-weighted structural brain imaging and morphometry at 7T using MP2RAGE," *PLoS One*, pp. 1–7, 2014, doi: 10.1371/journal.pone.0099676.

[20] G. D. Fullerton, J. L. Potter, and N. C. Dornbluth, "NMR relaxation of protons in tissues and other macromolecular water solutions," *Magn. Reson. Imaging*, pp. 209–226, 1982, doi: 10.1016/0730-725X(82)90172-2.

[21] J. P. Marques and R. Gruetter, "New Developments and Applications of the MP2RAGE Sequence - Focusing the Contrast and High Spatial Resolution R1 Mapping," *PLoS One*, vol. 8, pp. 1–11, 2013, doi: 10.1371/journal.pone.0069294.

[22] A. Ng, "The k-means clustering algorithm," in *Course CS229: Machine Learning*, 7AD, pp. 152–162.

[23] A. Coates and A. Y. Ng, "Learning feature representations with K-means," *Lect. Notes Comput. Sci. (including Subser. Lect. Notes Artif. Intell. Lect. Notes Bioinformatics)*, pp. 561–580, 2012, doi: 10.1007/978-3-642-35289-8-30.

[24] D. Arthur and S. Vassilvitskii, "K-means++: The advantages of careful seeding," in *Proceedings of the Annual ACM-SIAM Symposium on Discrete Algorithms*, 2007, pp. 1027–1035.

[25] M. A. Bernstein, K. F. King, and X. J. Zhou, *Handbook of MRI Pulse Sequences*. 2004.

[26] A. Tannús and M. Garwood, "Adiabatic pulses," in *NMR in Biomedicine*, 1997, pp. 423–434, doi: 10.1002/(SICI)1099-1492(199712)10:8<423::AID-NBM488>3.0.CO;2-X.

[27] M. Garwood and L. DelaBarre, "The return of the frequency sweep: Designing adiabatic pulses for contemporary NMR," *J. Magn. Reson.*, pp. 155–177, 2001, doi: 10.1006/jmre.2001.2340.

[28] G. Helms, J. Lätt, and H. Olsson, "Cross-vendor transfer and RF coil comparison of a high-resolution MP2RAGE protocol for brain imaging at 7T," *Acta Sci. Lund.*, vol. 001, pp. 1–15, 2020.

[29] M. Kadhim, "MP2RAGE simulations in Python," 2021. https://github.com/MustafaKadhim/MastersThesis/tree/main/Example.

[30] M. W. Woolrich *et al.*, "Bayesian analysis of neuroimaging data in FSL.," *Neuroimage*, 2009, doi: 10.1016/j.neuroimage.2008.10.055.

[31] M. Jenkinson, C. F. Beckmann, T. E. J. Behrens, M. W. Woolrich, and S. M. Smith, "Review FSL," *Neuroimage*, pp. 782–790, 2012.

[32] S. M. Smith, "Fast robust automated brain extraction," *Hum. Brain Mapp.*, pp. 143–155, 2002, doi: 10.1002/hbm.10062.

[33] J. P. Marques, "MP2RAGE Scripts - T1 map correction & Background noise removal."

[Online]. Available: https://github.com/JosePMarques/MP2RAGE-related-scripts.

[34] R. A. M. Haast, J. C. Lau, D. Ivanov, R. S. Menon, K. Uludağ, and A. R. Khan, "Effects of MP2RAGE B1+ sensitivity on inter-site T1 reproducibility and hippocampal morphometry at 7T," *Neuroimage*, pp. 1–11, 2021, doi: 10.1016/j.neuroimage.2020.117373.

[35] F. Eggenschwiler, T. Kober, A. W. Magill, R. Gruetter, and J. P. Marques, "SA2RAGE: A new sequence for fast B1+-mapping," *Magn. Reson. Med.*, pp. 1609–1619, 2012, doi: 10.1002/mrm.23145.

[36] G. E. Hagberg *et al.*, "Whole brain MP2RAGE-based mapping of the longitudinal relaxation time at 9.4T," *Neuroimage*, vol. 144, pp. 203–216, 2017, doi: 10.1016/j.neuroimage.2016.09.047.

[37] V. Wiggermann, I. M. Vavasour, S. H. Kolind, A. L. MacKay, G. Helms, and A. Rauscher, "Non-negative least squares computation for in vivo myelin mapping using simulated multi-echo spin-echo T2 decay data," *NMR Biomed.*, pp. 1–17, 2020, doi: 10.1002/nbm.4277.

[38] E. Cox and P. Gowland, "Measuring T2 and T2' in the brain at 1.5T, 3T and 7T using a hybrid gradient echo-spin echo sequence and EPI," *Proc. 16th Sci. Meet. Int. Soc. Magn. Reson. Med.*, 2008.

[39] Y. Zhang, M. Brady, and S. Smith, "Segmentation of brain MR images through a hidden Markov random field model and the expectation-maximization algorithm," *IEEE Trans. Med. Imaging*, pp. 45–57, 2001, doi: 10.1109/42.906424.

8 Appendix

8.1 Validation of simulations

T1 versus MP2RAGE plots, produced by our simulation tool, of published protocols such as the J. P. Marques et al [3] and R. A. M. Haast et al [34] (*Maastricht*) protocols (both based on the Bloch equations) is shown in Fig. (32). As observed, our produced simulations (A) display a similar output as in J. P. Marques et al [3] and R. A. M. Haast et al [34] (*Maastricht*) (B).

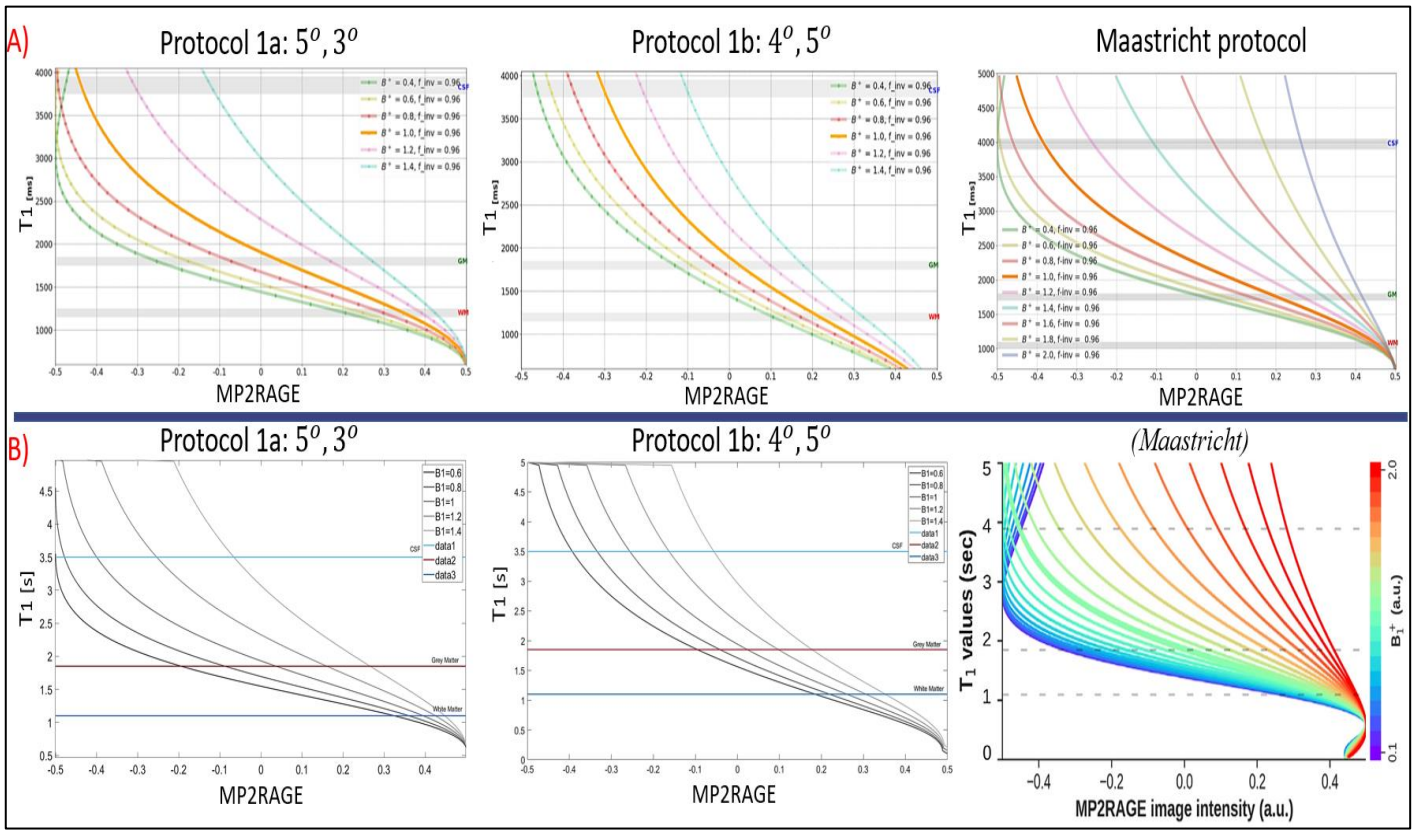

Fig.32. Produced simulations by our simulation tool (A) and published protocol output (B) by J. P. Marques et al [3] and R. A. M. Haast et al [34] (*Maastricht*). Apart from differences in the range of T1 and the more generous range of B_1^+-values in the Maastricht protocol, the plots look very similar.

8.2 K-means vs histogram thresholding

The results of segmentation for two different slices using the k-means method for different k-values are presented in Fig. (33). As shown, the higher the k-value the higher the number of classes the images are divided into. For the slice presented in (A), the k = 2 seems sufficient to obtain segmentation of WM. However, for the slice in (B), k=3 is considered to be a better value than k=2 for the segmentation of WM. This variation in the suitable k-value presents a challenge for acquiring reliable segmentation for all the tissues and slices.

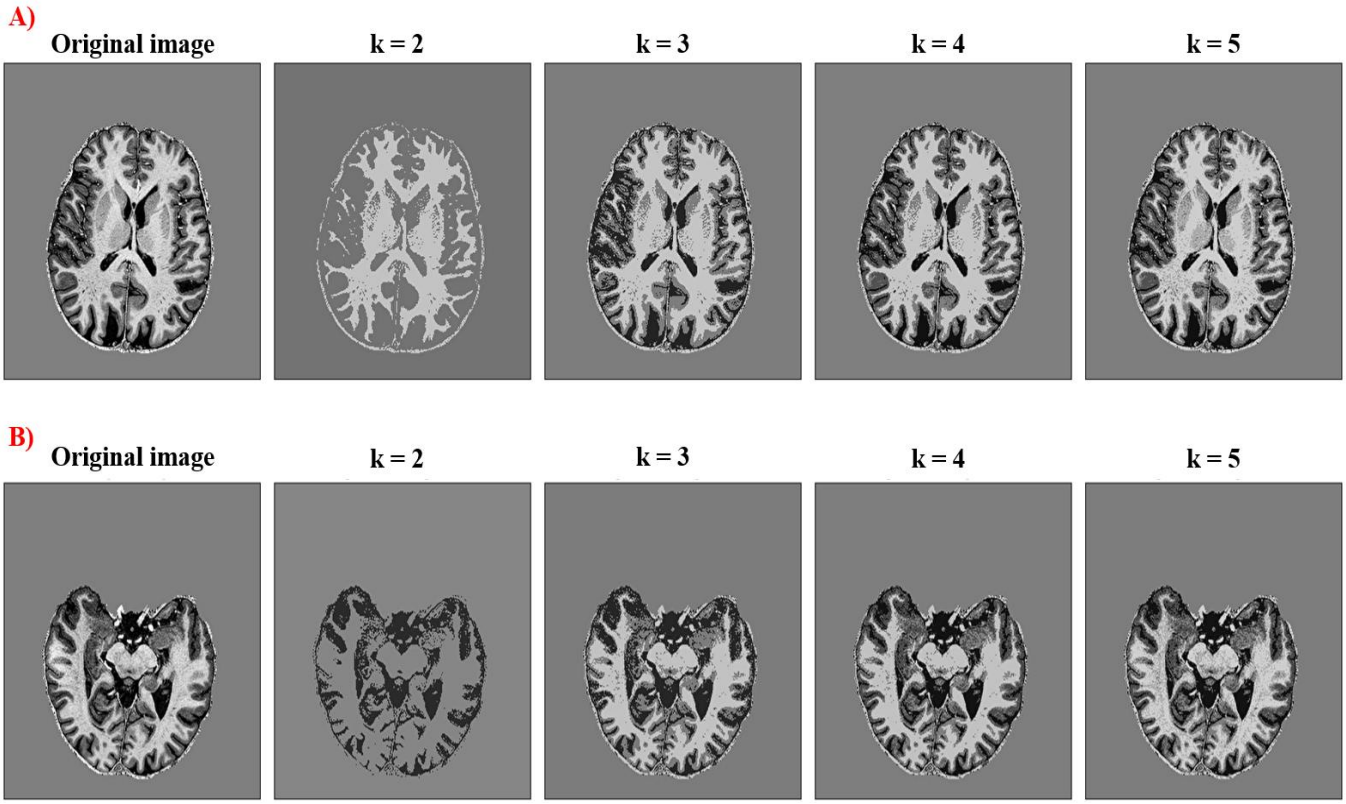

Fig. 33. Comparison of segmentation quality in different slices of the brain for different assigned k-values.

To compare the segmentation of WM in a selected brain slice with k-means and the histogram thresholding, a segmented sample is given in Fig. (34). The segmentation quality of WM appears relatively similar for k=3 and the threshold value, T=0.23 in an MP2RAGE image with intensity range [-0.5, 0.5].

Worth mentioning, that the FSL library contains a segmentation tool, FAST, that utilizes the k-means method to segment 3D images of the brain into different tissues (WM, GM, and CSF) [39]. In order to preform segmentation on ordinary images suffering from a spatial intensity bias (mainly due to B_1^- and B_1^+), FAST automatically determines an intensity bias field. The MP2RAGE images used in this work, should ideally be free of such bias. Thus, motivating segmentation by k-means alone.

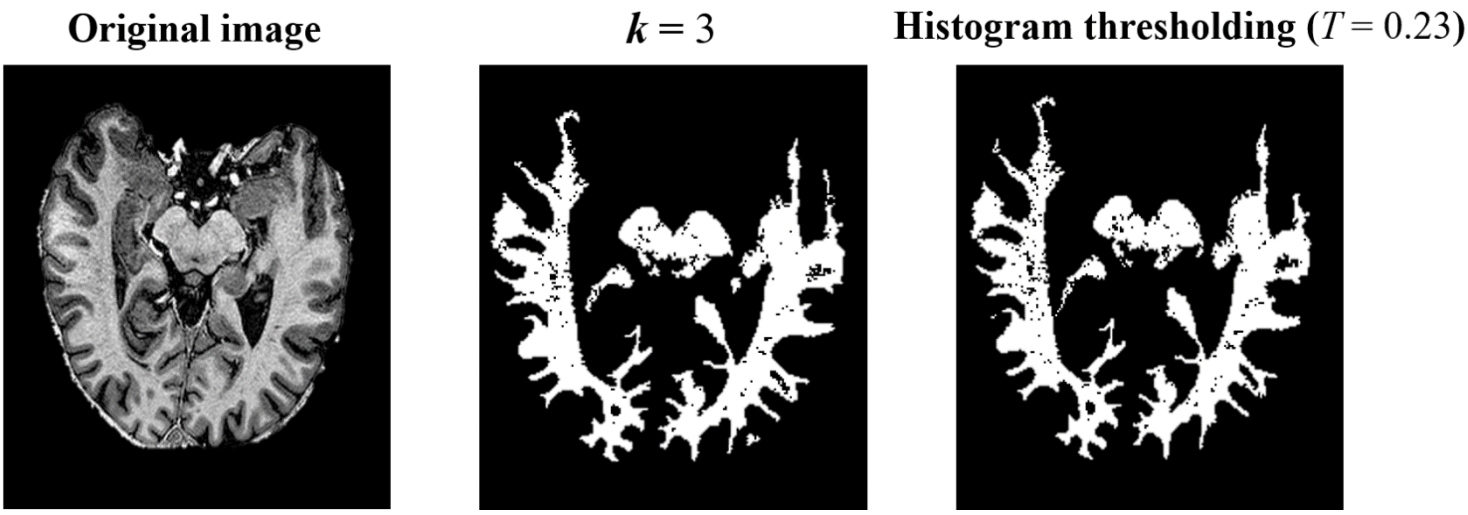

Fig. 34. Comparison of segmentation quality between the k-means and the histogram thresholding method for k = 3 and T = 0.23 in an MP2RAGE image with intensity range [-0.5, 0.5].

As observed, the histogram thresholding method yields comparable outcome as the unsupervised machine learning method, k-means. Additionally, histogram thresholding is a much simpler and computationally light method. The k-means method requires more knowledge/experience from the user to implement, due to the number of different variables it contains that influences the quality of the segmentation. Thus, for a quick and simple segmentation of WM, the histogram thresholding is recommended.